ASTRONOMY & ASTROPHYSICS
SUPPLEMENT SERIES

Astron. Astrophys. Suppl. Ser. **146**, 437–464 (2000)

Dust features in the 10-μm infrared spectra of oxygen-rich evolved stars

A.K. Speck[1], **M.J. Barlow**[2], **R.J. Sylvester**[2], **and A.M. Hofmeister**[3]

[1] Astronomy Department, University of Illinois at Urbana/Champaign, 1002 W. Green Street, Urbana, IL 61801, U.S.A.
e-mail: akspeck@astro.uiuc.edu
[2] Department of Physics and Astronomy, University College London, Gower Street, London WC1E 6BT, UK
[3] Department of Earth & Planetary Science, Washington University, St Louis, MO 63130, U.S.A.

Received December 22, 1999; accepted August 15, 2000

Abstract. We have analyzed the $8 - 13.5$ μm UKIRT CGS3 spectra of 142 M-type stars including 80 oxygen-rich AGB stars and 62 red supergiants, with a view to understanding the differences and similarities between the dust features of these stars. We have classified the spectra into groups according to the observed appearance of the infrared features. In each case the normalized continuum-subtracted spectrum has been compared to those of the other stars to find similarities and form groups. The dust features of the AGB stars are classified into six groups: *broad AGB*, where the feature extends from 8 μm to about 12.5 μm with little structure; *broad+sil AGB*, which consists of a broad feature with an emerging 9.7 μm silicate bump; and four *silicate AGB* groups in which a "classic" 9.7 μm silicate feature gets progressively narrower. Likewise, the supergiant spectra have also been classified into groups, however these do not all coincide with the AGB star groups. In the supergiant case we again have six groups: *featureless*, where there is little or no emission above the continuum; *broad Super*, where the feature extends from about 9 μm to about 13 μm; and four *silicate Super* groups, which again show a progression towards the narrowest "classic" 9.7 μm silicate feature. We compare the mean spectrum for each group, which yields two main results. Firstly, while the "classic" silicate feature is essentially identical for both AGB stars and red supergiants, the *broad* features observed for these two stellar types are quite different. We suggest that the dust in these two environments follows different evolutionary paths, with the dust around Mira stars, whose broad feature spectra can be fit by a combination of alumina (Al_2O_3) and magnesium silicate, progressing from this composition to dust dominated by magnesium silicate only, while the dust around supergiants, whose broad feature can be fit by a combination of Ca-Al-rich silicate and Al_2O_3, progresses from this initial composition to one eventually also dominated by magnesium silicate. The reason for the difference in the respective broad features is not clear as yet, but could be influenced by lower C/O ratios and chromospheric UV radiation fields in supergiant outflow environments. The second result concerns the $12.5 - 13.0$ μm feature discovered in IRAS LRS spectra and widely attributed to Al_2O_3. This feature is seen predominantly in the spectra of semiregular variables, sometime in Miras and only once (so far) in supergiant spectra. We argue that it is unlikely that this feature is due to Al_2O_3 or, as has more recently been suggested, spinel ($MgAl_2O_4$), but could be associated with silicon dioxide or highly polymerized silicates (not pyroxenes or olivines).

Key words: *(stars:)* circumstellar matter — stars: mass-loss — stars: AGB and post-AGB — *(stars:)* supergiants — infrared: stars — stars: variables: other

1. Introduction

1.1. Previous observation of dust around O-rich stars

In the late sixties, while investigating deviations of stellar energy distributions from blackbodies, Gillett et al. (1968) discovered a peak near 10 μm in the spectra of four late-type, evolved, variable stars. Woolf & Ney (1969) attributed this emission peak to circumstellar silicate grains around these stars. Since then there has been much interest in the exact nature of the dust around cool evolved stars, how this dust forms and the structure of the dust shells.

Hackwell (1972) suggested that the spectra of many M-stars were not consistent with the view that the circumstellar dust is comprised solely of silicate dust,

Send offprint requests to: A.K. Speck

implying that other constituents should be sought. Treffers & Cohen (1974) made high spectral resolution observations of oxygen-rich stars and concurred with Woolf & Ney (1969) on the attribution of the circumstellar dust features to silicates, however they did not preclude the inclusion of other grain types.

There have been various attempts to classify the different oxygen-rich dust features seen in the IRAS LRS spectra of evolved stars (e.g. Little-Marenin & Little 1990; hereafter LML90, Sloan & Price 1995; hereafter SP95). LML90 have classified the variation in the spectral features from M-type AGB stars into six categories: featureless, broad, 3 component, sil++ (a "9.7 μm" feature with a strong feature on its long wavelength side centered at about 11.3 μm), sil+ (a stronger "9.7 μm" feature with a weaker long wavelength feature) and sil (a strong "9.7 μm" silicate feature). They suggested that there is an evolutionary sequence in the spectral features, starting with a featureless continuum, then developing a broad feature, followed by a three component feature, a two component feature and finally increasingly strong silicate features. Following this work, SP95 devised another classification system and found that they could categorize the spectra into eight groups which formed a smooth progressive sequence from broad feature to "classic" silicate emission. This classification system involved examining the fluxes at 10, 11 and 12 μm (F_{10}, F_{11} and F_{12}), and comparing the ratios of the fluxes, rather than a visual inspection of the feature shapes. Where their finding differed from those of LML90 was with respect to the 12.5 − 13.0 μm feature. They found that this feature was apparent in approximately 40−50% of the spectra across all groups. Therefore, if the sequence is evolutionary, the 12.5 − 13.0 μm feature is due to a dust-type whose formation is not related to dust evolution.

Sloan et al. (1996) continued this work on the IRAS LRS database and found that the 12.5 − 13.0 μm feature was present primarily in the spectra of semiregular variables (SRs): 75 − 90% of SRb variables exhibit the feature, while only 20 − 25% of Miras exhibit this feature. Other than this strong tendency to be found in the spectra of SRb variables, the 12.5 − 13.0 μm feature was not found to be related to any peculiarities that would distinguish the sources.

Onaka et al. (1989) had attributed the broad 12.5 μm band seen in the spectra of some O-rich stars (see Hackwell 1972 and Vardya et al. 1986) to alumina (Al_2O_3). They also found that fits to nearly all their M star spectra could be improved by the inclusion of Al_2O_3 grains. They suggested that the only way to form the silicate grains was for them to grow on pre-existing grains of Al_2O_3 which act as seed nuclei. However, for most polytypes of Al_2O_3, the infrared feature peaks at ∼11.5 − 12.0 μm rather than 12.5 − 13.0 μm. One polytype, α-Al_2O_3 (or corundum), has a peak in the right wavelength range, but also exhibits a feature at ∼21 μm which is not seen in the LRS spectra. Therefore, Al_2O_3 seems unlikely to be the cause of the 12.5 − 13.0 μm band seen in these spectra. This conclusion was supported by the work of Begemann et al. (1997), who suggested that the 12.5 − 13.0 μm band is probably associated with silicates.

Justtanont et al. (1998) observed strong emission lines, attributed to CO_2, in the ISO-SWS spectra of stars which exhibit the 12.5 − 13.0 μm feature. Their data showed that the strengths of the CO_2 emission lines and the 12.5 − 13.0 μm feature are well correlated, implying that these features originate in the same region of the circumstellar envelope. Justtanont et al. (1998) asserted that the occurrence of correlated CO_2 and 12.5 − 13.0 μm emission is indicative of a warm (∼650 − 1250 K) gas layer close to the star where the carriers of these features are formed. They also suggested that an increase in mass-loss would provide a mechanism to prevent formation and/or excitation of the CO_2.

Posch et al. (1999) used ISO-SWS data to characterize the observed 12.5 − 13 μm feature and then compared this to the spectra of various appropriate minerals. They suggested that spinel ($MgAl_2O_4$) is the most likely candidate. The attribution of the 12.5 − 13.0 μm feature to this mineral is discussed in more detail in Sect. 3.

Although much the focus of recent research has been on the nature of the 12.5 − 13.5 μm emission feature, a number of other papers have focussed more on the general silicate features. Sloan & Price (1998; hereafter SP98) extended their previous LRS dataset (SP95) to include supergiants and S-stars. They found that the majority of supergiants fell into the "classic" silicate groups defined for AGB stars. There was little evidence for supergiants with the broad feature. How their findings compare to the current work will be discussed later.

Sylvester et al. (1994, 1998) discovered the presence of 8.6– and 11.3 μm "UIR" emission bands (usually attributed to carbon-rich material, e.g. polycyclic aromatic hydrocarbons) superposed on the silicate emission features of a number of M supergiant stars, particularly amongst members of the h&χPersei double cluster. Such UIR-band emission was not found in the spectra of any AGB stars. Sylvester et al. attributed this stark contrast in emission properties to the presence of a chromospheric UV radiation field around the M supergiants, capable of dissociating the CO molecules which would otherwise have locked up most of the available carbon atoms in the circumstellar outflows. PAH molecules might then form from the liberated carbon atoms, and be fluorescently excited to emit in the IR by the ambient UV photons. Sylvester et al. only detected UIR-band emission from intermediate luminosity supergiants which had relatively broad silicate bands. The non-detectability of any UIR-band emission in their spectra of more luminous supergiants could be due to smothering of the UV photon field in the denser winds of these stars, or to lack of contrast of the bands against the much stronger silicate emission features of these stars.

Sylvester (1999) investigated the 10 μm spectra of a number of oxygen-rich evolved stars whose IRAS LRS spectra had been classified as showing SiC 11 μm band emission. Using UKIRT CGS3 spectra with higher S/N and spectral resolution, he found that two of these stars, both supergiants, instead showed 11.3 μm UIR-band emission superposed on silicate features. The remainder showed standard 3-component O-rich dust features, with peaks at 10, 11 and 13 μm, apart from one object with a self-absorbed silicate feature. There is therefore currently no evidence for SiC emission features in the spectra of any O-rich evolved stars.

1.2. Dust formation around oxygen-rich evolved stars

Scenarios for the formation of dust grains in circumstellar shells around oxygen-rich stars have been investigated by several groups over the last thirty years. It seems appropriate to discuss the types of dust grains that these models predict to appear in order to constrain our own attributions.

The first attempts to predict the types of grains that should be expected to form in these environments neglected the actual nucleation processes and concentrated on the chemistry (e.g. Gilman 1969 and references therein). The first investigation of dust formation processes in terms of nucleation and grain growth was by Salpeter (1974) who concluded that grain formation proceeded by nucleation of small refractory seed grains (i.e. oxides) onto which an "onion-layer" mantle of the more abundant silicates could form. Since then the basic premise of grain nucleation and growth has remained the same (e.g. Sedlmayr 1989; Jeong et al. 1999), but the details change and the exact nature of the expected condensates is still being debated.

Pégourié & Papoular (1985) discussed the grain-types expected in circumstellar shells. Their model, based mainly on models of condensation in the solar nebula, implied that the precise nature of the grains formed is determined by the elemental composition and oxidation properties of the parent atmosphere, along with the density structure of the dust shell. According to their model: 1) the concentration of iron in silicates is always expected to be low (mole % Fe_2SiO_4(fayalite) $\sim$ 20%; and $FeSiO_3$ $\sim$ 10%); 2) Mg_2SiO_4(forsterite) forms before $MgSiO_3$ (enstatite) in a cooling atmosphere, but forsterite is converted into enstatite by gas-solid reaction with SiO. They did not expect the dust to be pure forsterite or even forsterite with some ($\leq$ 20%) fayalite. Disequilibrium calculations showed that the dust shells of M-stars should also contain SiO_2, solid (metal) Fe, Ca_2SiO_4 and Al_2O_3.

Stencel et al. (1990) hypothesized the formation of "chaotic silicate". In their scenario, a chaotic silicate forms from a supersaturated vapour containing metal atoms, SiO, AlO and OH in a hydrogen atmosphere. Inside the chaotic silicate, where both silicon and aluminium are less than fully oxidized, the higher reducing potential of Al would initially act to produce Al-O bonds at the expense of Si-O bonds. Thus, the stretching modes of solid, amorphous alumina would grow at the expense of the 9.7 μm Si-O stretch associated with silicates. However, Si and O are approximately ten times more abundant than Al and therefore once the aluminium is completely oxidized, the Si and SiO components of the grain should begin to oxidize and thus increase the strength of the classic 9.7 μm silicate band.

Tielens (1990) reviewed the thermodynamic and kinetic factors which go into determining which grain species form in O-rich circumstellar environments. This was taken to be the "classic" condensation sequence and fits with the basic ideas of grain nucleation and growth presented here. This will be discussed in more detail in Sect. 4.

In a more recent paper, Kozasa & Sogawa (1997, 1998) suggested that seed nuclei are alumina (Al_2O_3) grains, so that the first dust grains that form would be "naked" Al_2O_3 grains. These refractory grains can exist relatively close to the star. Further out, where the temperature allows formation of lower temperature condensates, these Al_2O_3 grains would act as seed nuclei and become coated with silicates. Such core-mantle grains would have a minimum size of $\sim$150 nm. This is very similar the Salpeter (1974) model. However, Kozasa & Sogawa also suggested that, even further from the star, homogeneous silicate nucleation can occur, so that there would be a population of very small (a few nanometres) pure silicate grains. They suggested that the classic 10 μm silicate feature is due to these very small grains while the core-mantle Al_2O_3-silicate grains are responsible for the $12.5 - 13$ μm feature. We will return to this question in Sect. 3.

The utilisation of Al_2O_3 grains as seed nuclei was called into question by Jeong et al. (1999) who suggested that alumina is unlikely to be present in the gas phase and therefore could not be used to build the "critical cluster" that constitutes a seed nucleus. However, Gail & Sedlmayr (1999) state that the relevant information needed to establish this is not available for alumina. Jeong et al. (1999) used TiO_2 as their nucleation seed material, after finding that it was thermodynamically and chemically the most favoured refractory species (see Gail & Sedlmayr 1998). Their models suggested that the first dust species to form, closest to the star, would be aluminium silicates ($Al_6Si_2O_{13}$), a result not found in other models. They also found that titanium-bearing dust should form. However, Ti is over thirty times less abundant than Al and 400 times less abundant than Mg, Si, and Fe, which probably precludes the formation of detectable quantities of Ti-rich dust. At somewhat lower temperatures, Jeong et al. expected Mg_2SiO_4 (forsterite), $MgSiO_3$ (enstatite) and SiO_2 to form. At even lower temperatures they predicted that iron oxides should form and eventually contribute $\sim$30% of the dust volume, contrary to the

Lodders & Fegley (1999) statement that "stars do not rust".

Gail & Sedlmayr (1999) predicted that M-star circumstellar shells should contain several different dust species. Their models, like those of Jeong et al. (1999), start with TiO_2 cluster formation; however, as mentioned above, Gail & Sedlmayr did not exclude the possibility of Al_2O_3 seed nuclei. They found the most abundant condensate to be olivine. The exact Fe/Mg ratio could vary and they even suggested that this ratio changes as the grain grows, so that there could be a gradient in the Fe/Mg ratio across the grains. They also found that metallic iron particles form (in agreement with Lodders & Fegley), as well as MgO (periclase) and a very small amount of SiO_2 material.

It is clear from the models discussed above that there is not a consensus as to the nature of the dust grains that form around O-rich stars. However, the models do provide insight into whether some dust species are at all plausible. The aim of the present paper is to compare and contrast the mid-infrared features found in the spectra of cool evolved O-rich stars. To this end, mid-infrared UKIRT CGS3 spectra have been obtained that have a significantly higher signal to noise ratio and a somewhat higher spectral resolution than those available in the IRAS LRS database, although the $7.5 - 13.5$ μm spectral coverage of these ground-based spectra is more restricted than the $7.5 - 22$ μm coverage of the IRAS LRS. We aimed in particular to determine whether any dust feature types are associated with particular types of star, and what can be learned from the differences in spectral features amongst the various stellar types.

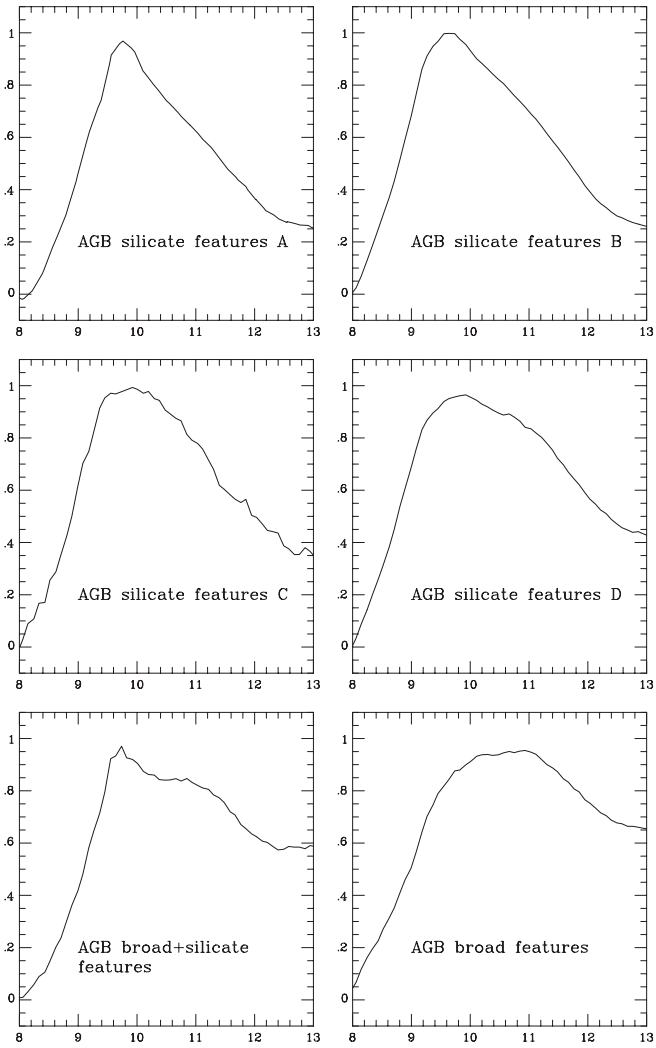

Fig. 1. Mean spectra for each of the AGB star groups – progressing between the broadest feature (bottom right) and the narrowest silicate feature (top left)

2. The observational investigation

We present here a survey of dust features present in the mid-IR spectra of 80 oxygen-rich AGB stars and 62 M-supergiants, with a view to identifying similarities and differences between the features amongst these various types of stars. The selection of targets was largely dictated by their accessibility to the 3.8-m UKIRT on Mauna Kea at the dates of several different observing runs. The AGB stars were observed mainly during two runs, in May 1991 and October 1992, although RW And and RZ Ari were observed in October 1990 and SX Cyg was observed in November 1993. The supergiant stars were observed over a wider range of dates, from October 1992 to June 1998. The supergiant spectra from October 1992 and August 1995 have already been published by Sylvester et al. (1994, 1998). They are included here because they are used for a different purpose to that of Sylvester et al.

The nature of our survey means that these are snapshot spectra, obtained at a random phase of the stellar pulsation cycle. Work by Little-Marenin et al. (1996), Creech-Eakman et al. (1997) and Monnier et al. (1998) has indicated that AGB star silicate emission bands can vary systematically as a function of pulsation cycle, primarily in the strength of the feature but sometimes also in its profile. However, these observed profile variations have in general been significantly less pronounced than the differences between the emission feature types that are classified here.

2.1. Observations

Observations were taken using the 3.8-m United Kingdom Infrared Telescope (UKIRT) with the common-user spectrometer CGS3 (see Cohen & Davies 1995). We obtained $7.5 - 13.5$ μm spectra with a 5.5-arcsec circular aperture, and a spectral resolution of 0.17 μm. Two grating settings gave a fully sampled 64-point spectrum. Wavelength calibration was with respect to observations of a Kr arc-lamp.

Table 1. AGB stars observed

Source	IRAS names	Other names	Variability Type*	Spectral Type	Observation Date	Calibrator	8.0 μm flux (10^{-12} Wm^{-2} μm^{-1})
Y Cas	00007+5524	IRC+60001, HD 225082	M	M7e	Oct. 5 '92	ϵCyg	5.46
T Cet	00192-2020	IRC-20007, AFGL 53, HD 1760	SRb	M5/M6I/II	Nov. 1 '93	βPeg	10.0
T Cas	00205+5530	IRC+60009, AFGL 57, HD 1845	M	M7e	Oct. 5 '92	ϵCyg	21.3
RW And	00445+3224	IRC+30015, AFGL 109, HD 4489, CIT 2	M	S6,2e	Oct. 5 '90	αTau	1.97
SAO 37673	01556+4511	IRC+50049, AFGL 278, HD 11979	SR?	M7	Oct. 4 '92	αCet	12.8
o Cet	02168-0312	Mira, IRC+00030, AFGL 318, HD 14386	M	M7IIIe	Oct. 6 '92	αLyr	185
R Cet	02234-0024	IRC+00032, AFGL 4195, HD 15105	M	M4e	Oct. 4 '92	αCMa	1.01
RR Per	02251+5102	IRC+50062, AFGL 335, HD 15186	M	M6e-M7e	Oct. 7 '92	αCet	3.20
RZ Ari	02530+1807	IRC+20051	SRb	M6III	Oct. 5 '90	αTau	7.94
RT Eri	03318-1619	IRC-20043, AFGL 500, HD 22228	M	M7e	Oct. 4 '92	αTau	5.42
IK Tau	03507+1115	IRC+10050, AFGL 529, NML Tau	M	M6e	Oct. 7 '92	αCet	138
V Eri	04020-1551	IRC-20049, AFGL 542, HD 25725	SRc?	M5/M6IV	Oct. 4 '92	αTau	7.48
W Eri	04094-2515	IRC-30033, AFGL 552, HD 26601	M	M7e	Oct. 4 '92	αCma	2.13
BX Eri	04382-1417	IRC-10075, AFGL 615	SR	M3	Oct. 4 '92	αCMa	3.23
R Cae	04387-3819	AFGL 617, HD 29844	M	M6e	Oct. 4 '92	αCMa	3.72
TX Cam	04566+5606	IRC+60150, AFGL 664	M	M9	Oct. 4 '92	αCma	14.3
UX Aur	05121+4929	IRC+50138, HD 33877	SR	M4(II)	Oct. 4 '92	αCet	0.988
R Aur	05132+5331	IRC+50141, AFGL 715	M	M7	Oct. 4 '92	αCet	13.2
X Ori	05351-0147	IRC+00080, AFGL 786	M	M8	Oct. 7 '92	αAur	3.26
RU Aur	05367+3736	IRC+40135, AFGL 794	M	M8e	Oct. 7 '92	αAur	3.99
SZ Aur	05384+3854	IRC+40136, AFGL 802, HD 37645	M	M8e	Oct. 7 '92	αAur	2.51
U Aur	05388+3200	IRC+30126, AFGL 822, HD 37724	M	M7e	Oct. 7 '92	αAur	6.33
RT Lep	05404-2342	IRC-20077, AFGL 8105	M	M9e	Oct. 4 '92	αCMa	2.05
S Col	05450-3142	IRC-30049	M	M6e	Oct. 4 '92	αCMa	1.30
CH Pup	06434-3628	AFGL 1008	M	Me	Oct. 7 '92	αCet	2.28
AZ Mon	06551+0322	IRC+00140,	M	M6e	Oct. 7 '92	αCet	1.26
GX Mon	06500+0829	AFGL 1028	M	M9	Oct. 7 '92	αCet	9.32
Y Lyn	07245+4605	IRC+50180, AFGL 1120, HD 58521	SR	M6S	May 24 '91	αBoo	5.40
Z Pup	07304-2032	IRC-20123, AFGL 1140, HD 60218	M	M4-M9e	Oct. 6 '92	αCma	4.97
DU Pup	07329-2352	IRC-20134, AFGL 1151	M	M	Oct. 6 '92	αCMa	5.21
U Pup	07585-1242	IRC-10184, AFGL 1215, HD 65940	M	M5e-M8e	Oct. 6 '92	αCma	1.88
RS Cnc	09076+3110	IRC+30209, AFGL 1329, HD 78712	SR	M6S	May 25 '91	αBoo	25.4
R Leo	09448+1139	IRC+10215, AFGL 1380, HD 84748	M	M8e	May 22 '91	αBoo	67.4
R Hya	13269-2301	IRC-20254, AFGL 1627, HD 117287	M	M7e	May 25 '91	αBoo	57.8
W Hya	13462-2807	IRC-30207, AFGL 1650, HD 120285	SRa	M8e	May 21 '91	αBoo	152
RX Boo	14219+2555	IRC+30257, AFGL 1706, HD 126327	SRb	M7.5e	May 24 '91	αBoo	25.8
S CrB	15193+3139	AFGL 4990S, HD 136753	M	M7e	May 24 '91	αBoo	7.08
RU Her	16081+2511	IRC+30283, AFGL 1832, HD 145459, CIT 8	M	M7e	May 24 '91	αBoo	8.74
U Her	16235+1900	IRC+20298, AFGL 1858, HD 148206	M	M7e	May 24 '91	αBoo	12.6
BG Her	17072+1844	IRC+20314,	M	M3	May 24 '91	βPeg	0.948
V1692 Sgr	18320-1918		M	M9	Oct. 7 '92	βPeg	0.813
V1111 Oph	18349+1023	IRC+10365, AFGL 2206	M	M9	Oct. 4 '92	αLyr	11.0
X Oph	18359+0847	IRC+10360, AFGL 2213, HD 172171	M	M5e-M9e	Oct. 4 '92	αLyr	13.2
V2059 Sgr	18501-2132		M	M8	Oct. 4 '92	αLyr	2.92
R Aql	19039+0809	IRC+10406, AFGL 2324, HD 177940	M	M7e	Oct. 6 '92	αLyr	16.0
AG Sgr	19044-2856	IRC-30403, HD177868	M	M5-M6e	Oct. 7 '92	βPeg	0.619
V342 Sgr	19093-3256	IRC-30404, AFGL 5556	M	M9	Oct. 5 '92	βPeg	4.29
W Aql	19126-0708	IRC-10497, AFGL 2349	M	S6,6e	Oct. 7 '92	βPeg	65.2
Z Sgr	19167-2101	IRC-20555, HD 181060	M	M5e	Oct. 5 '92	βPeg	2.02
V635 Aql	19343+0912		M	?	Oct. 7 '92	βAnd	0.252
BG Cyg	19369+2823	IRC+30379, AFGL 2426	M	M7e	Oct. 4 '92	αLyr	2.45
V462 Cyg	19384+4346	IRC+40355, AFGL 2429	M	M7e	Oct. 4 '92	αLyr	1.15
RR Sgr	19528-2919	IRC-30419, AFGL 5569, HD 188378	M	M5e	Oct. 7 '92	βPeg	4.76
Z Cyg	20000+4954	IRC-50314, HD 190163	M	M5e	Oct. 5 '92	βPeg	1.88
SX Cyg	20135+3055	IRC+30423, HD 192788	M	M7e	Nov. 2 '93	αLyr	1.30
RU Cap	20296-2151	IRC-20590	M	M9e	Oct. 7 '92	βAnd	0.533
Y Del	20392+1141	IRC+10475	M	M8e	Oct. 7 '92	βAnd	1.87
Y Aqr	20417-0500	IRC-10546	M	M6.5e	Oct. 7 '92	βPeg	1.36
W Aqr	20438-0415	IRC+00489	M	M7	Oct. 7 '92	βAnd	1.95
RZ Cyg	20502+4709	IRC+50347	SRa	M7	Oct. 5 '92	βPeg	3.71
UW Cep	20581+5841	IRC+60301	M	M8	Oct. 5 '92	βPeg	1.34
UU Peg	21286+1055	IRC-10498, AFGL 2775	M	M7e	Oct. 7 '92	ϵCyg	6.76
RU Cyg	21389+5405	IRC+50390, AFGL 2790, HD 206483	SRa	M8e	Oct. 5 '92	βPeg	9.46
EP Aqr	21439-0226	IRC+00509, AFGL 2806, HD 207076, SAO 145652	SRb	M8	Oct. 6 '92	αLyr	20.3
YY Cep	22000+5643	IRC+60337	M	M6	Oct. 5 '92	βPeg	1.04
SV Peg	22035+3506	IRC+40501, AFGL 2845, HD 209872	SRb	M7	Oct. 7 '92	ϵCyg	9.47
CU Cep	22097+5647	IRC+60345, AFGL 2865	SRb	M5	Oct. 5 '92	βPeg	4.99
R Peg	23041+1016	IRC+10527, AFGL 3023, HD 218292	M	M7e	Oct. 5 '92	βPeg	10.8
V Cas	23095+5925	IRC+60389, HD 218997	M	M5.5e	Oct. 5 '92	βPeg	3.67
BU And	23212+3927	IRC+40536, AFGL 3088	M	M7e	Oct. 6 '92	βPeg	4.41
R Aqr	23412-1533	IRC-20642, AFGL 3136, HD 222800	M	M7e	Oct. 6 '92	αLyr	32.2
Z Cas	23420+5618	IRC+60418, AFGL 3141, HD 222914	M	M7e	Oct. 7 '92	ϵCyg	3.56
R Cas	23558+5196	IRC+50484, AFGL 3188, HD 224490	M	M7e	May 21 '91	αBoo	41.5

*Variability Type: M = Mira; SR = semi-regular variable.
T Cet and V Eri are italicized because it is unclear whether each star is a giant or a supergiant – see Sect. 2.2.

Table 2. Supergiant stars in the sample

Source	IRAS names	Other names	Variability Type*	Spectral Type	Observation Date	Calibrator	8 μm flux in 10^{-12} Wm^{-2} μm^{-1}
MZ Cas	00186+5940	IRC+60008,	Lc	M1.3Iab	Oct. 5 '92	ϵ Cyg	1.25
BD+47485	01400+4815	IRC+50043, HD 10465	Lc?	M2Ib	Aug. 16 '95	β And	0.660
BD+58342	01550+5901	IRC+60070, HD 236915	??	M2.4Ib	Aug. 16 '95	β And	0.433
XX Per	01597+5459	IRC+50052, HD 12041	SRc	M3.6Ib	Oct. 6 '92	β Peg	2.58
KK Per	02068+5619	IRC+60074, HD 13136	Lc	M1.9Ib	Oct. 7 '92	α Cet	0.889
V550 Per	02116+5754	HD 13658	??	M5.4Iab	Oct. 7 '92	α Cet	0.274
BU Per	02153+5711	IRC+60078	SRc	M3.7Ib	Oct. 4 '92	α Tau	0.705
T Per	02157+5843	IRC+60079, HD 14142	SRc	M2.1Iab	Oct. 4 '92	α Tau	0.400
V506 Cas	02167+5926	IRC+60081, HD 14242	??	M5.7Iab	Oct. 7 '92	α Cet	0.591
AD Per	02169+5645	IRC+60082, HD 14270	SRc	M2.4Iab	Oct. 4 '92	α Tau	0.771
FZ Per	02174+5655	IRC+60083, HD 14330	Lc	M0.3Iab	Oct. 7 '92	α Cet	0.521
PR Per	02181+5738	IRC+60085, HD 14404	Lc	M0.7Iab	Oct. 7 '92	α Cet	0.552
SU Per	02185+5622	IRC+60086, HD 14469	SRc	M3.3Ib	Oct. 4 '92	α Tau	1.12
RS Per	02188+5652	IRC+60087, HD 14488	SRc	M4.4Ib	Oct. 6 '92	β Peg	1.33
S Per	02192+5821	IRC+60088, HD 14528, AFGL 323	SRc	M4.5Iab	Oct. 4 '92	α Tau	6.81
V439 Per	02196+5658	BD+56595	??	M5.8Iab	Oct. 7 '92	α Cet	0.368
V441 Per	02217+5712	IRC+60090, HD 14826	??	M3.1Iab	Oct. 7 '92	α Cet	0.929
YZ Per	02347+5649	IRC+60093, HD 236979	??	M1.9Iab	Oct. 7 '92	α Cet	0.976
GP Cas	02360+5922	IRC+60094, AFGL 359	Lc	M2.8Iab	Aug. 16 '95	β And	0.983
V648 Cas	02473+5738	HD 237010, BD+57647	??	M2.9Iab	Aug. 16 '95	β And	1.01
IO Per	03030+5532	IRC+60110	Lc	M3I	Oct. 4 '92	α Tau	4.88
AH Sco	17080-3215	IRC-30282, HD 155161	SRc	M5I	Aug. 16 '95	η Sgr	14.0
IRC-30312	17374-3156		??	M2.6Ia	Aug. 16 '95	η Sgr	1.68
KW Sgr	17488-2800	IRC-30326, HD 3167486, AFGL 2017	SRc	M2.4Ia	Aug. 16 '95	η Sgr	3.50
V540 Sgr	17566-3555	HD 163869	Lc	M5Iab	Aug. 16 '95	η Sgr	1.10
VX Sgr	18050-2213	IRC-20431, AFGL 2071, HD 165674	SRc	M5-M6I	Oct. 4 '92	βPeg	73.3
IRC-10419	18227-1347		??	M2.5Iab	Aug. 17 '95	γ Aql	0.450
UY Sct	18248-1229	IRC-10422, AFGL 2162	SRc	M3.4Iab	Jun. 27 '98	γ Aql	3.72
HD 171094	18305-1408	IRC-10435, AFGL 2186	??	M3I	Aug. 17 '95	γ Aql	0.875
UW Aql	18550+0023	IRC+00398	Lc	M2.2Iab	Jun. 27 '98	γ Aql	0.945
V1302 Aql	19244+1115	IRC+10420, AFGL 2390	??	F8I	Oct. 6 '92	α Lyr	18.2
IRC-20565	19272-1929		??	M2Ib	Aug. 17 '95	γ Aql	0.285
NR Vul	19480+2447	IRC+20438, HD 339034	Lc	M1.1Iab	Aug. 16 '95	γ Aql	2.46
BC Cyg	20197+3722	IRC+40409, AFGL 2560	Lc	M3.2Iab	Aug. 16 '95	γ Aql	7.47
KY Cyg	20241+3811	IRC+40415, AFGL 2575	Lc	M3.9Iab	Aug. 16 '95	γ Aql	6.95
AZ Cyg	(20h56m)	IRC+50351, AFGl 2683	??	M3.1Iab	Aug. 16 '95	γ Aql	2.26
AZ Cep	22069+5918	IRC+60343, AFGL 2857	Lb	M1.6I	Aug. 16 '95	β Peg	0.480
ST Cep	22282+5644	IRC+60357, AFGL 2916, HD 239978	Lc	M2.6Ia	Aug. 17 '95	β Peg	1.01
U Lac	22456+5453	IRC +50446, HD 215924, AFGL 2957	SRc	M2.5Ia	Aug. 17 '95	β Peg	2.95
V355 Cep	22471+5902		??	M1.1Iab	Aug. 16 '95	β Peg	0.442
V358 Cas	23281+5742	IRC+60410, AFGL 3110	Lc	M2.8Ia	Aug. 16 '95	β And	1.42

*Variability Type: L = irregular variable; SR = semi-regular variable.

Table 3. 10 μm classifications of AGB stars

featureless AGB	*broad AGB*	*broad+sil AGB*	*silicate AGB* A	*silicate AGB* B	*silicate AGB* C	*silicate AGB* D
BU And	AG Sgr	BX Eri	CU Cep	DU Pup	IK Tau	CH Pup
R Hya	BG Cyg	RR Per	RS Cnc	GX Mon	R Aqr	R Cae
R Peg	R Aql	RW And	RU Cyg	R Cet	RT Lep	R Cas
RZ Ari	R Aur	RX Boo	U Her	RU Cap	RU Aur	W Eri
T Cas	R Leo	RZ Cyg	UU Peg	S CrB	RU Her	Y Aqr
UX Aur	RR Sgr	SAO 37673	X Ori	U Aur	EP Aqr	
V Cas	RT Eri	UW Cep	Mira	V1111 Oph	TX Cam	
	S Col	V462 Cyg		V342 Sgr	U Pup	
	SZ Aur	W Aqr		V635 Aql	V2059 Sgr	
	V1692 Sgr	Y Cas		Z Cyg	Y Del	
	W Aql	Z Cas		Z Pup	Y Lyn	
	W Hya	SV Peg			Z Sgr	
	YY Cep	AZ Mon				
	V Eri					
	X Oph					

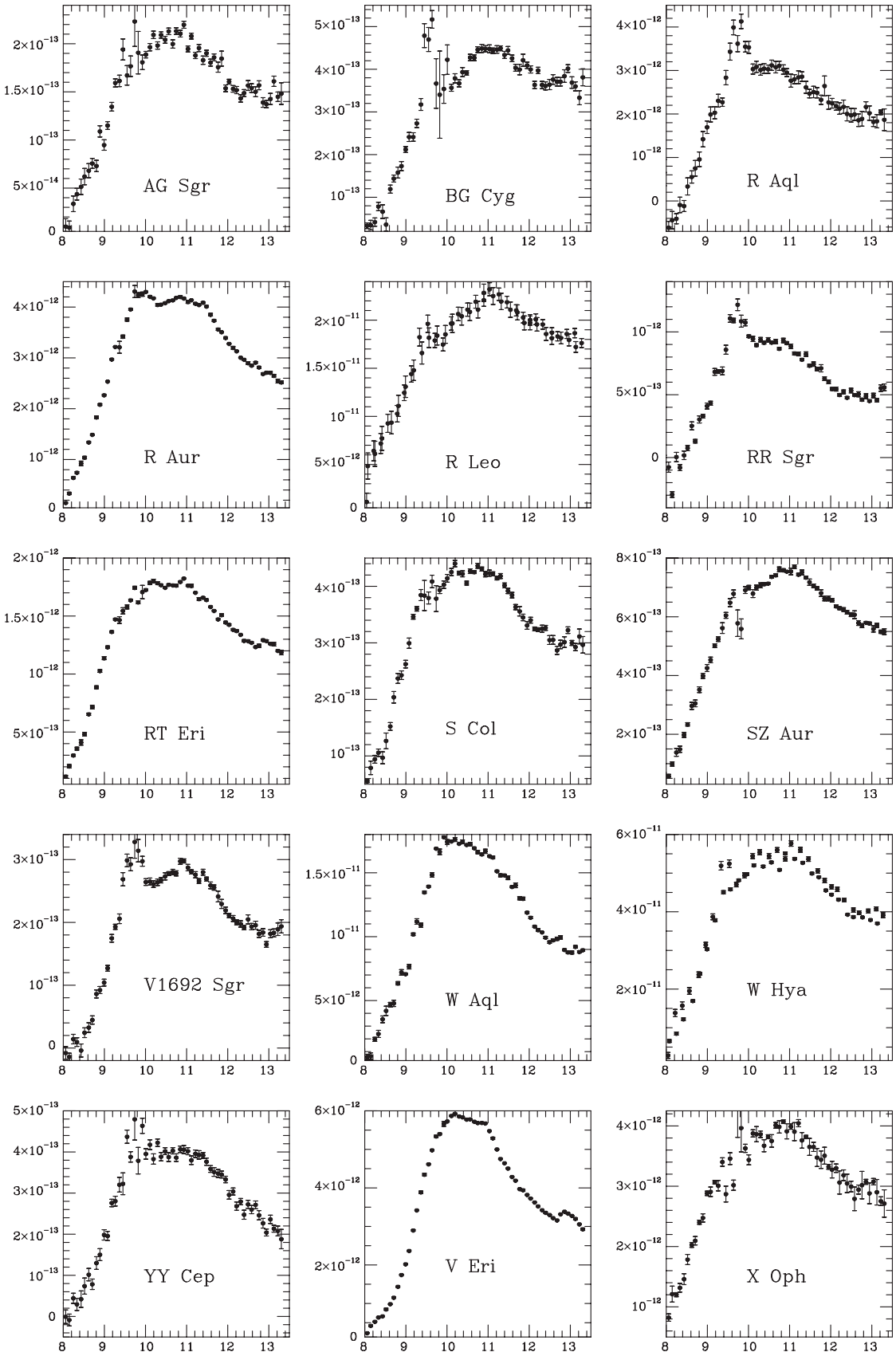

Fig. 2. Continuum-subtracted AGB star spectra classed as showing *broad* features. x-axis is wavelength in μm. y-axis is flux in W m^{-2} μm^{-1}

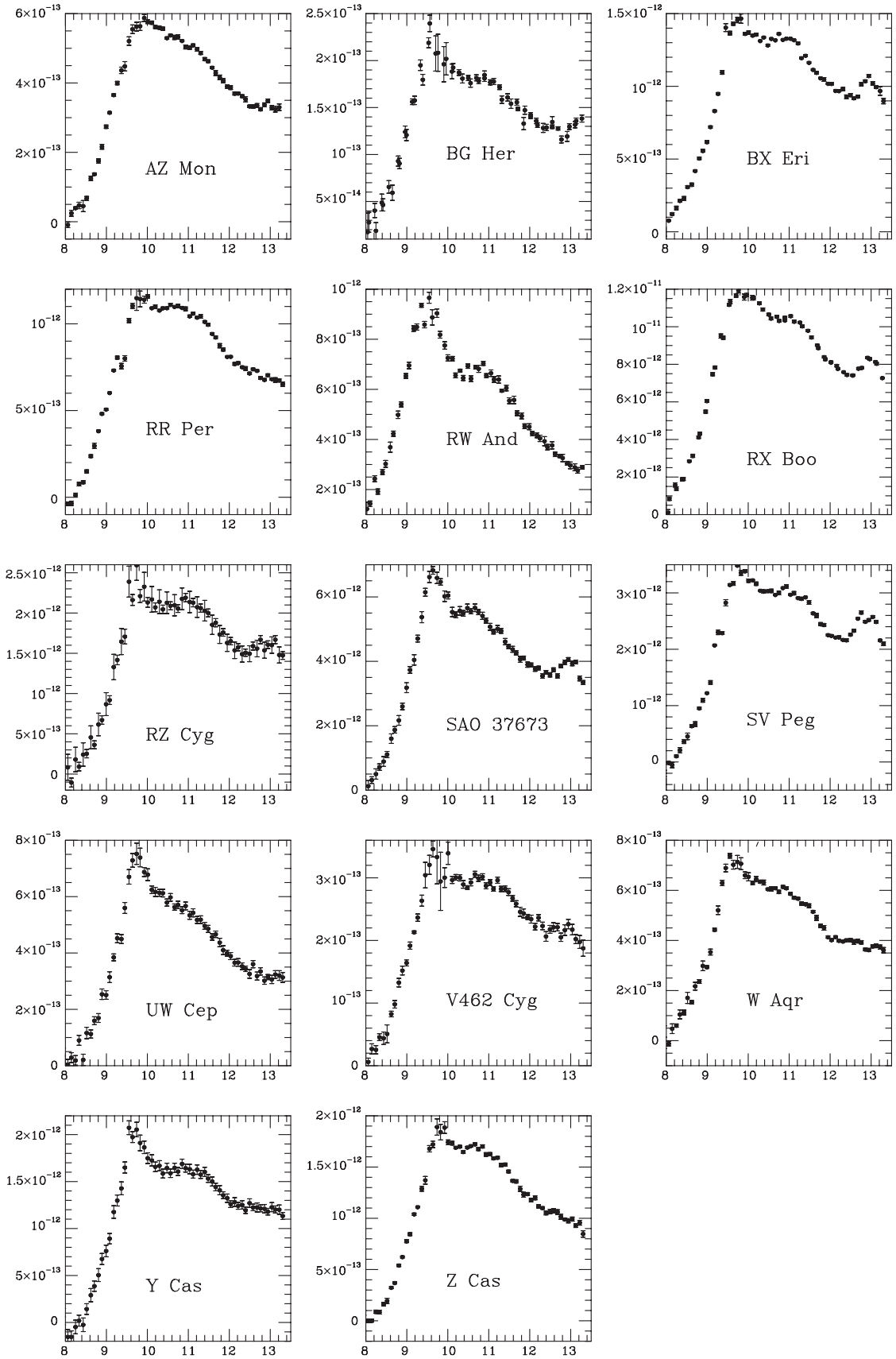

Fig. 3. Continuum-subtracted AGB star spectra classed as showing *broad+sil* features. x-axis is wavelength in μm. y-axis is flux in W m^{-2} μm^{-1}

Table 4. 10 μm classifications of supergiant stars

broad Super A	*broad Super* B	*silicate Super* 1	*silicate Super* 2	*silicate Super* 3	*silicate Super* 4
AD Per	BD+58342	AH Sco	AZ Cyg	AZ Cep	V1302 Aql
FZ Per	V439 Per	KW Sgr	BC Cyg	V648 Cas	IRC-30312
V506 Per	V550 Per		BU Per	GP Cas	S Per
PR Per			HD 171094	IRC-10419	UY Sct
V441 Per			IRC-20565	KY Cyg	VX Sgr
T Per			ST Cep	MZ Cas	
KK Per			V358 Cas	NR Vul	
BD+47485			V540 Sgr	RS Per	
			XX Per	SU Per	
			YZ Per	UW Aql	
				V355 Cep	

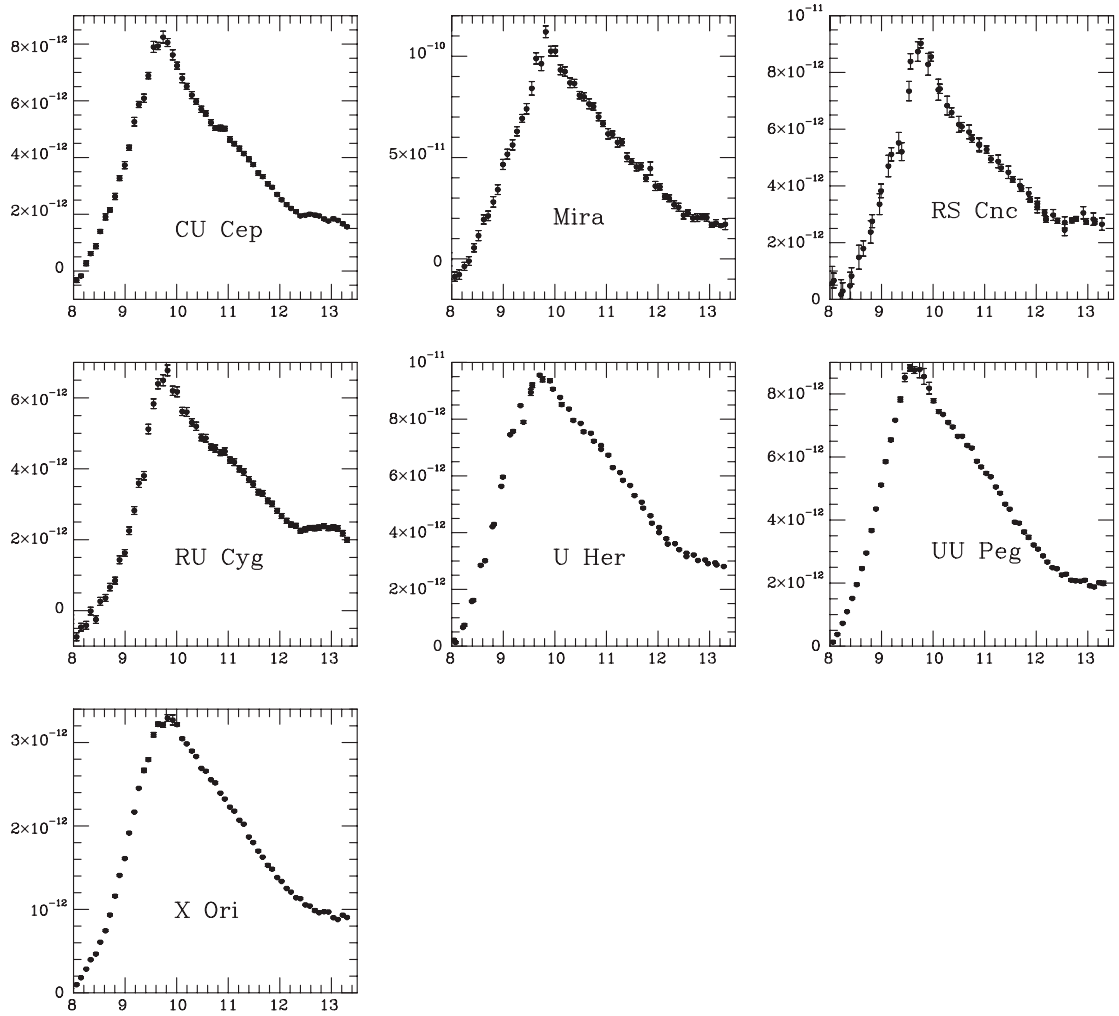

Fig. 4. Continuum-subtracted AGB star spectra classed as showing group A *silicate* features. x-axis is wavelength in μm. y-axis is flux in W m^{-2} μm^{-1}

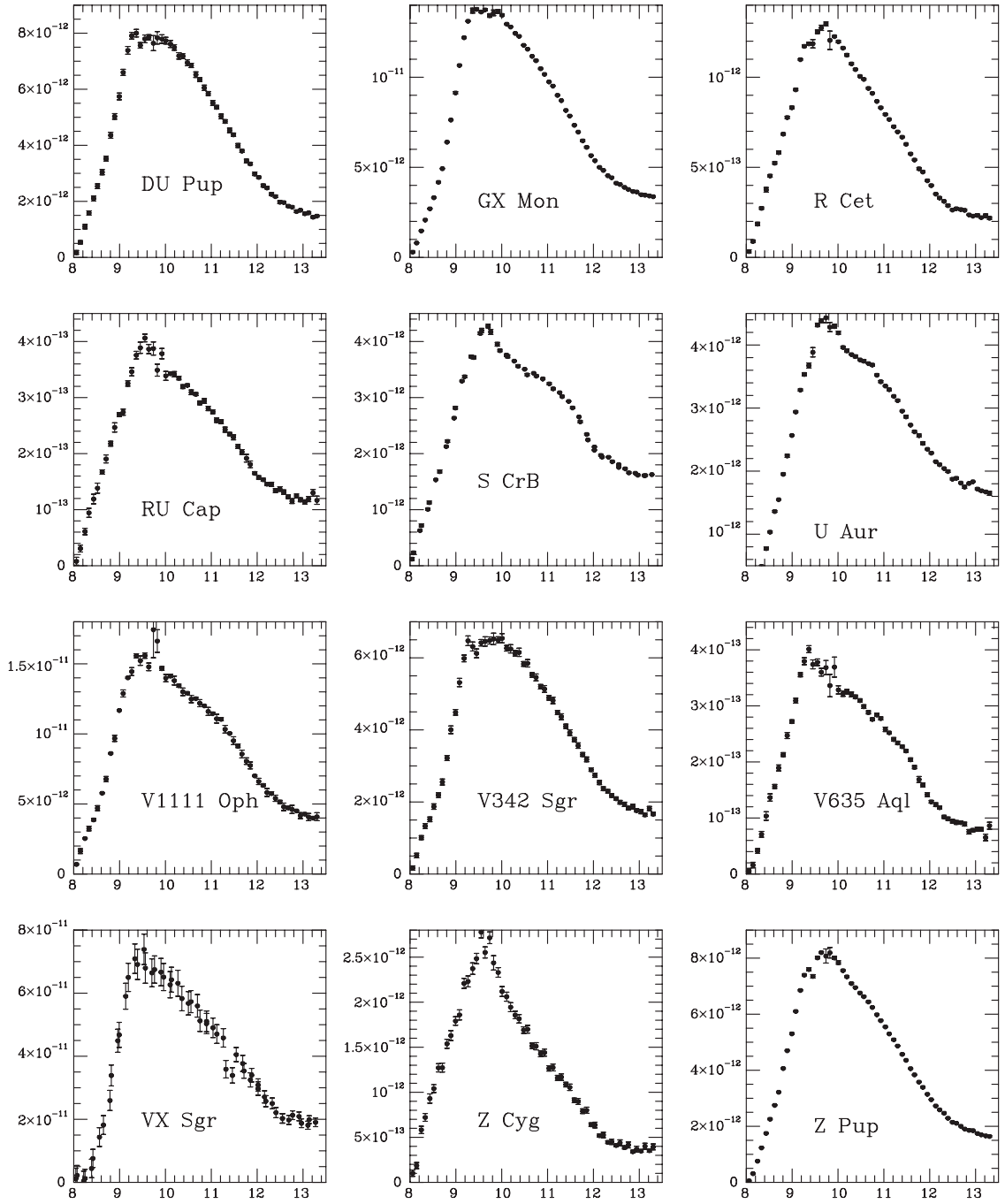

Fig. 5. Continuum-subtracted AGB star spectra classed as showing group B *silicate* features. x-axis is wavelength in μm. y-axis is flux in W m^{-2} μm^{-1}

The telescope secondary was chopped east-west at 5 Hz using a 30-arcsec throw. The error bars in the plots represent 1σ standard errors on the fluxes. Due to imperfect cancelation of the time-varying atmospheric ozone band, the error bars are larger at approximately 9.6 μm. Details of the observed stars can be found in Table 1 for the AGB stars and Table 2 for the supergiants.

2.2. Classifying the features

For each source in our sample a 3000 K blackbody representing the stellar photosphere was normalized to the spectrum at 8.0 μm. This was then subtracted from the observed astronomical spectrum to yield the spectra that are plotted in Figs. 2–8 and 10–14. Since the mean level of the spectra between 7.5 and 8.0 μm is zero and the error bars are larger because of greater atmospheric absorption

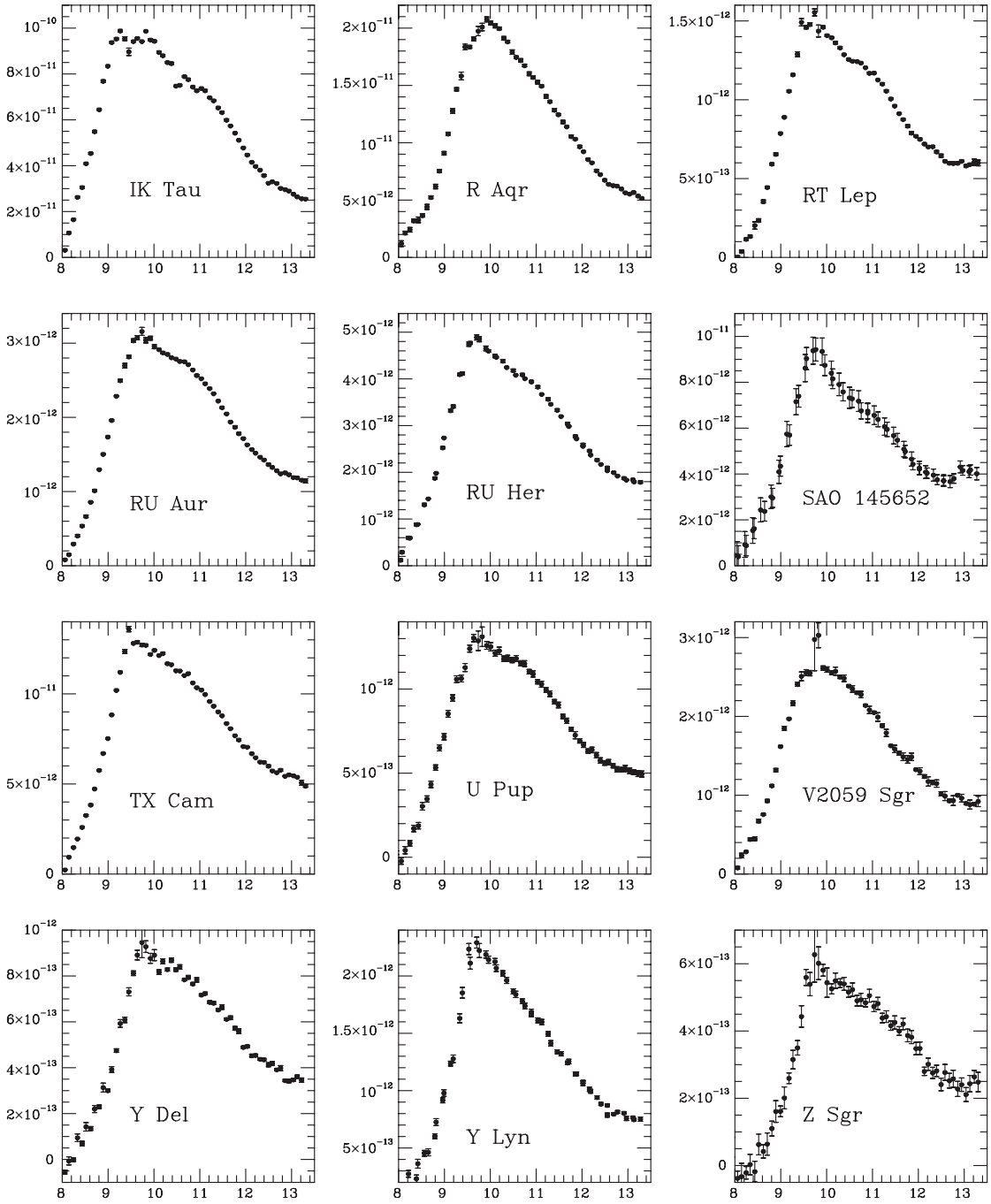

Fig. 6. Continuum-subtracted AGB star spectra with group C *silicate* features. x-axis is wavelength in μm. y-axis is flux in W m^{-2} μm^{-1}

between these wavelengths, we have only plotted our continuum-subtracted spectra from 8.0 μm onwards. Our continuum subtraction procedure implicitly assumes that the 8.0 μm continuum is dominated by blackbody-like stellar photospheric emission, i.e. that neither continuum dust emission nor gaseous SiO fundamental-band emission or absorption is important. Higher resolution spectra of the SiO fundamental and first overtone bands (e.g. Tsuji et al. 1997; Waters et al. 1999; Aringer et al. 1999) indicate that the gaseous SiO band is not likely to have significantly perturbed our low resolution spectra. A much more detailed modeling of wide spectral coverage ISO-SWS spectra would be needed to investigate whether continuum dust emission in general makes a significant contribution at 8 μm. However, the ISO-SWS spectra of Tsuji et al. (1997) indicate that for high mass loss stars, such as the

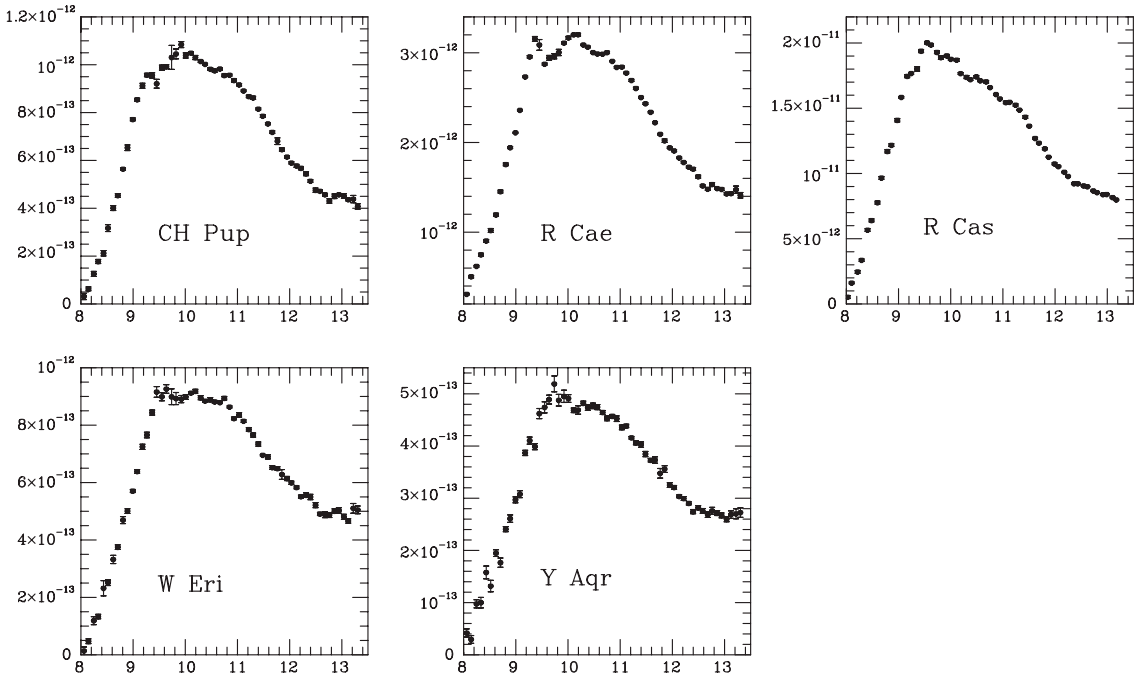

Fig. 7. Continuum-subtracted AGB star spectra classed as showing group D *silicate* features. x-axis is wavelength in μm. y-axis is flux in W m^{-2} μm^{-1}

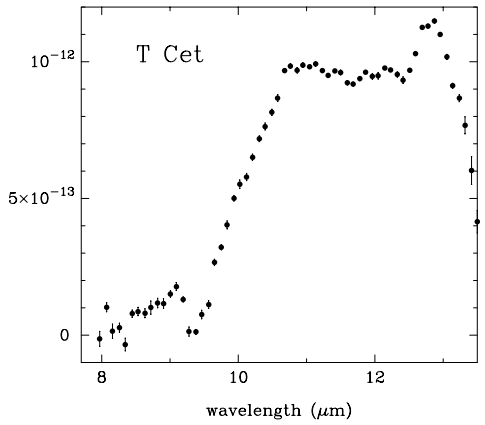

Fig. 8. The continuum-subtracted spectrum of T Cet. x-axis is wavelength in μm. y-axis is flux in W m^{-2} μm^{-1}

supergiant S Per, continuum dust emission is significant at 8 μm but that for lower mass loss rate stars (the majority of our sample) the contribution from continuum dust emission at this wavelength is much less pronounced.

In producing our continuum-subtracted spectra (CSS), we have assumed that the photospheric temperature for each star is 3000 K. However, we find that varying the adopted blackbody temperature by ±1000 K about the adopted 3000 K has very little effect on the shape and strength of the derived continuum-subtracted dust features, since we are in the Rayleigh-Jeans domain of the photospheric Planck distributions. Therefore the exact effective temperatures of the stars, within the natural scatter that is expected for these stars, should not affect our data analysis.

In order to aid comparisons between different spectra, we also produced normalized "continuum-subtracted spectra" (CSS) for the AGB stars and supergiants in our sample, by normalizing the CSS to a peak flux of unity. The normalized CSS of each AGB star was compared to those of the other AGB stars to find similarities and form groups. Leaving aside the seven AGB stars in our sample whose individual spectra show no pronounced emission features (classed as "featureless" in Table 3), the dust features of the AGB stars have been classified into three groups: *broad AGB*, where the feature extends from 8 μm to about 12.5 μm with little structure; *broad+sil AGB*, which consists of a broad feature with an emerging 9.7 μm silicate bump; and *silicate AGB*, which is the "classic" 9.7 μm silicate feature. In addition, the *silicate AGB* group can be classified further into four subgroups, A, B, C, D, which show slightly differently shaped silicate features, as shown by the mean spectra. These variations seem to show a sequence from broader to narrower silicate feature. The stars in each group are summarized in Table 3, and the mean feature profile for each group is shown in Fig. 1. The original CSS are shown in Figs. 2−7, grouped in the classes described above.

The *broad+sil AGB* groups can also be split into two groups according to whether the spectra show the 12.5 − 13.0 μm feature. This will be discussed later.

Two of our sources, T Cet and V Eri, have been classified both as AGB stars and as supergiants in various

published works. For this reason, exactly whether these stars should be included in the AGB star groupings or the supergiant groupings is ambiguous. In fact T Cet has been classified as an AGB star (e.g. Bedding & Zijlstra citeB98), a supergiant (e.g. SP98), M-star (e.g. Bedding & Zijlstra 1998), MS-star (e.g. Groenewegen & de Jong 1998) and S-star (e.g. Skinner et al. 1990; Groenewegen 1993). This source also has a markedly different spectrum from any others in the sample (e.g. Speck 1998; Skinner et al. 1990). We can see in Fig. 8 that the spectral features for this source are unlike any others in our sample and it therefore needs to be treated separately. For this reason, T Cet was removed from the sample. V Eri has variously been classed as an AGB star and as a supergiant (see e.g. Hashimoto 1994; Habing 1996; Neri et al. 1998; Triglio et al. 1998; Cernicharo 1998 etc.). Kwok et al. (1997) give V Eri the spectral classification M6II, i.e. intermediate between a giant and a supergiant, while Houk & Smith-Moore (1988) assign V Eri a spectral class of M5/M6IV, which would make it a subgiant. Furthermore, V Eri exhibits the 12.5 − 13.0 μm feature, which is seen in many AGB star spectra but only in one other supergiant spectrum (that of S Per; see Sect. 3). We have therefore placed it in the AGB grouping, rather than in the supergiant grouping.

In the same way as for the AGB stars, the normalized CSS of each supergiant was compared to those of the other supergiants to find similarities and form groups. The dust features of the supergiant stars can also be classified into three basic groups: *featureless*, whose emission above the continuum is weak and hard to classify; *broad Super*, where the feature extends from ∼9 μm to ∼13 μm; and *silicate Super*, which again is the "classic" 9.7 μm silicate feature. Since the *featureless* spectra show little of interest regarding dust they will not be discussed further here. The *broad* feature can be classified into two further subgroups, one extending from 9 to 13 μm, and one with a short wavelength onset at 9.5 μm. The difference between these two *broad* groups may be entirely due to differences in the underlying dust continuum. Examination of the silicate features in these spectra is slightly compromised by the appearance of UIR bands (see Sylvester et al. 1994, 1998). The strong 11.3 μm UIR band has been edited out of the averaged spectra shown in Fig. 9. Again, the "classic" silicate group (*silicate Super*) can be classified further into four subgroups, 1, 2, 3 & 4, where the exact shapes of the silicate features vary slightly and the averages show this. One supergiant with a silicate feature, U Lac, did not fit into any of these four groups, but does have the basic silicate feature and matches group B from the AGB star classifications. The stars in each group (excluding *featureless*) are summarized in Table 4, the mean feature from each group is shown in Fig. 9, and the original CSS are shown in Figs. 10−14, grouped in the classes described above.

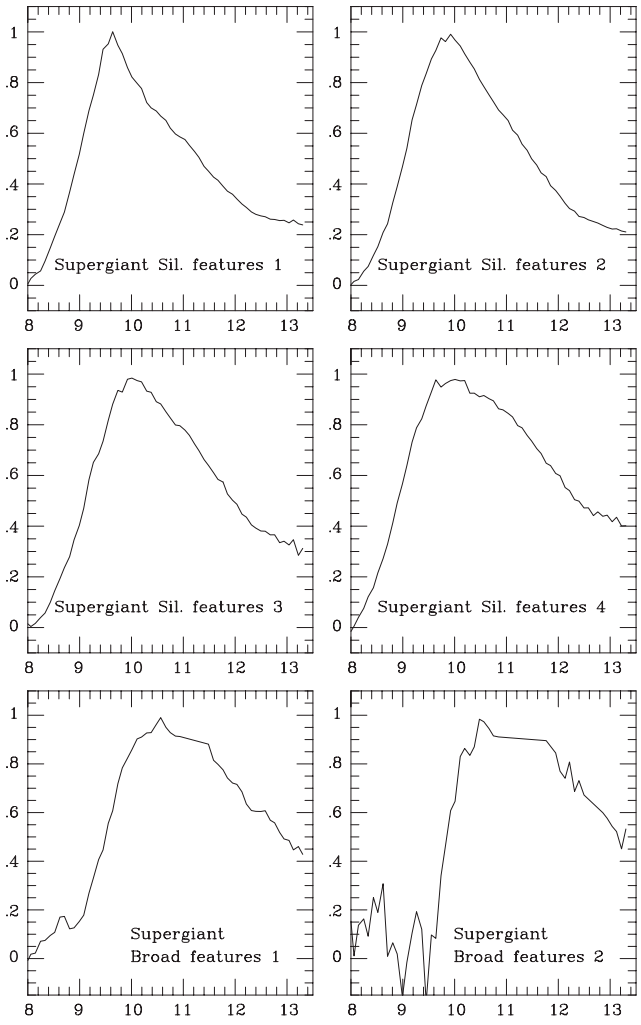

Fig. 9. Mean spectra for each of the supergiant star groups - progressing between the broadest feature (bottom right) and the narrowest silicate feature (top left)

Our classifications of AGB stars and supergiant can be compared to those of SP95 and SP98. These comparisons are shown in Tables 5 and 6. The classification system used by SP95 & SP98 gives each spectrum a number: SE1 to SE8, where SE1 refers to the *broad* feature; the SE number increases as the silicate feature emerges up to SE8 which refers to the "classic" narrow silicate feature. We would therefore expect spectra in the our *broad* feature class to have low SE numbers. As we progress through the classes up to the narrow silicate feature class, the SE number should increase. In general we concur with the SP95 and SP98 progression, as can be seen in Tables 5 and 6. However, there are a couple of spectra for which the classifications are markedly different: W Hya, which we class as having a broad feature while SP95 give it a strong silicate feature; and R Cae, which we class as *silicate D* and they give a broad feature class. These differences may be due to their classification method, which only uses

relative fluxes at 10, 11 and 12 μm rather than the overall shape of the features. However, in comparing the classifications used we found that none of the stars that we have classified as *broad Super* appear in their dataset and they do not have any examples of the broad feature. This is unfortunate, since it appears to be one of the few ways in which the observed dust features differ between AGB stars and supergiants.

2.3. Comparing dust features from AGB stars and supergiants

Having classified the spectra into groups, we have compared the spectral features for AGB stars and supergiants.

2.3.1. The "classic" silicate feature

Amongst both the AGB and supergiant classes we have distinguished sub-groupings of the "classic" silicate feature. Comparing these sub-groups, we find that the various silicate features found in the spectra of AGB stars are very similar to those found in the spectra of supergiants. Figures 15a−d shows the comparisons of the various silicate features. In each case the mean AGB silicate feature for each sub-group is plotted along with the closest matching supergiant silicate features. Figure 15a compares AGB silicate group A with two supergiant silicate groups (1 & 2). The AGB feature is found to match the average of these two supergiant features. Figure 15b shows AGB silicate group B, together with the spectrum of the unclassified supergiant U Lac. Figure 15c shows AGB silicate group C with two supergiant silicate groups (3 & 4). As with AGB silicate group A, this AGB group appears to be intermediate between the two supergiant groups. Figure 15d shows AGB silicate group D with the supergiant group 4. It is clear from these figures that, although the silicate feature varies from star to star, similar shaped features are present in the spectra of both AGB stars and supergiants, and seem to form a progression between broader and "classic" narrow 9.7 μm silicate features.

2.3.2. The *broad* feature

As we can see from Fig. 16, the *broad* AGB star feature is quite different from the two *broad* supergiant features. The *broad* features for supergiants are slightly narrower than for AGB stars, extending from 9.0 − 9.5 μm to ∼13 μm, rather than 8 − 12.5 μm as in the AGB star spectra. Furthermore, the flux continues to drop longward of 12.5 μm, rather than leveling off as in the case of the AGB stars. In addition, the *broad* feature for AGB stars seems to develop a silicate peak on its way to becoming a "classic" silicate feature (see *broad+sil* classification; Fig. 1); this does not happen in the supergiant spectra. Only one supergiant in the sample, S Per (see Fig. 14), exhibits the 12.5 − 13.0 μm feature seen in some AGB star spectra and this may be due to this star's unusual characteristics. It is believed that S Per is a relatively new supergiant and that its dust shell is thinner and more spherically symmetric than is usually found for supergiants (Richards 1997; Richards et al. 1999). These characteristics make the dust shell more like that of a semiregular red giant than a supergiant and may explain the appearance of the 12.5 − 13.0 μm feature in its spectrum.

2.4. The featureless spectra

Those AGB and supergiant 8 − 13 μm excess spectra which have been labeled as "featureless" are all very weak compared to the local stellar photospheric continua. Signal to noise considerations may therefore be largely responsible for the inability to classify these excess spectra. To test this, we co-added the five AGB star 8 − 13 μm excess spectra labeled as "featureless" in Table 5. The resulting mean spectrum had better S/N and resembled the broad AGB star feature discussed above. It may therefore be the case that the respective broad features are responsible for the low-contrast "featureless" spectra of AGB stars and supergiants.

3. The ∼13 μm feature in AGB star spectra

As discussed above, there is virtually no evidence for the 12.5 − 13.0 μm feature in supergiant spectra. It is, however, clearly present in some AGB star spectra (see Figs. 2−7; see also the ISO-SWS observations of Posch et al. 1999) and requires further investigation. The 12.5 − 13 μm feature is not ubiquitous amongst the AGB star spectra. In our sample, this feature is found rarely in the spectra which exhibit a broad feature extending from 8.5 to 12 μm, sometimes in spectra with the "classic" silicate feature, and is most regularly found in the spectra that combine the broad and silicate features, although it is still not universal. The AGB star spectra in the *broad+sil* group, where the 12.5 − 13.0 μm feature is most frequently seen, have been divided further into those spectra which exhibit the 12.5 − 13.0 μm feature, and those which do not. The mean features of these two subgroups are plotted together in Fig. 17a, where the 12.5 − 13.0 μm feature is clearly seen. In Fig. 17b, we have subtracted the mean of the *broad+sil* spectra which do not exhibit the 13.0 μm feature from the mean of those spectra that do, in order to isolate this feature. From this we have found the peak position of the mean 12.5 − 13 μm feature to be 12.92 μm. This is very close to the position measured by Posch et al. (1999), 12.95 − 13.05 μm, although is notably on the short wavelength side of their measurement.

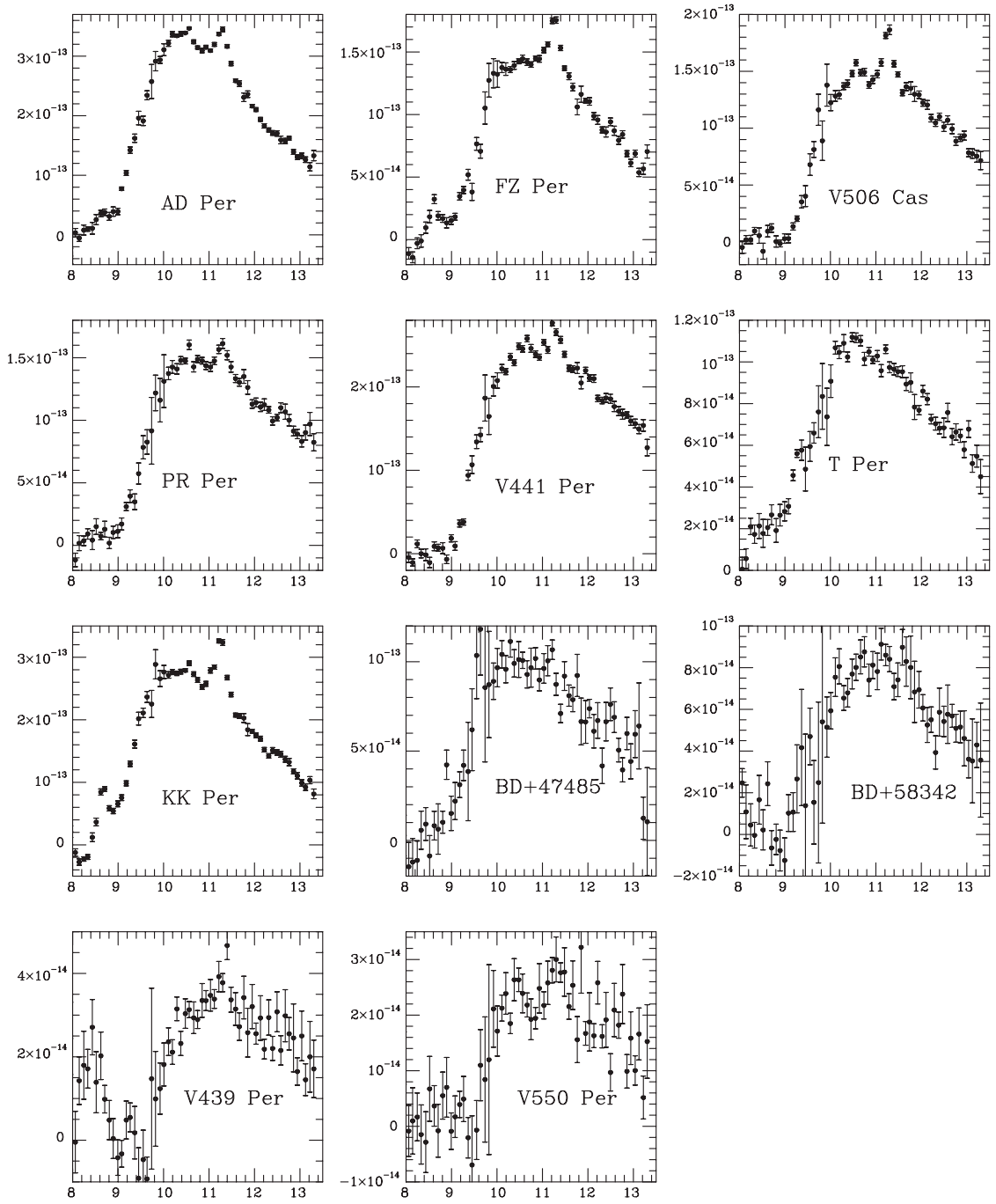

Fig. 10. Continuum-subtracted supergiant spectra classed as showing *broad* features. x-axis is wavelength in μm. y-axis is flux in W m^{-2} μm^{-1}

This discrepancy may be due to the feature's proximity to the long wavelength limit of our observed spectra, which may have caused the loss of a small portion on the long wavelength side of the feature. This would also account for the smaller full width half maximum (FWHM) of our mean 12.5 − 13 μm feature of 0.45 μm, compared to the FWHM for this feature of 0.5 − 0.8 μm measured by Posch et al. (1999) in their higher resolution SWS spectra spectra of 11 stars. Their mean spectrum shows the feature to have a pronounced long-wavelength asymmetry, which could however be largely due to CO_2 and other narrow emission features which are present in this wavelength region of their spectra.

If we look for differences between the stars which exhibit the 13 μm feature, and those which do not, we find that, within the *broad+sil* group, all the stars with the feature are non-Mira semi-regular variables, whereas those stars without the feature are all Miras (see Table 7).

Table 5. Comparing classifications - AGB star features

Source	Variability Type	Our Class	SP95 Class	Source	Variability Type	Our Class	SP95 Class
BU And	M	featureless	SE2	CH Pup	M	*silicate D*	SE4
R Hya	M	featureless	SE2t	R Cae	M	*silicate D*	SE3
R Peg	M	featureless	SE4	R Cas	M	*silicate D*	SE5
T Cas	M	featureless	SE1	W Eri	M	*silicate D*	SE6
V Cas	M	featureless	SE1	Y Aqr	M	*silicate D*	SE4
BG Cyg	M	*broad*	SE2t	IK Tau	M	*silicate C*	SE5
R Aql	M	*broad*	SE5	R Aqr	M	*silicate C*	SE6
R Leo	M	*broad*	SE2	RT Lep	M	*silicate C*	SE6
RR Sgr	M	*broad*	SE4	RU Aur	M	*silicate C*	SE8
RT Eri	M	*broad*	SE3	RU Her	M	*silicate C*	SE5
S Col	M	*broad*	SE2	EP Aqr	SR	*silicate C*	SE4
SZ Aur	M	*broad*	SE2t	TX Cam	M	*silicate C*	SE5
W Aql	M	*broad*	SE3	U Pup	M	*silicate C*	SE6
W Hya	SR	*broad*	SE8	Y Lyn	SR	*silicate C*	SE8
YY Cep	M	*broad*	SE4	Z Sgr	M	*silicate C*	SE6
V Eri	SR	*broad*	SE3t	DU Pup	M	*silicate B*	SE5
X Oph	M	*broad*	SE1	GX Mon	M	*silicate B*	SE6
RR Per	M	*broad+sil*	SE2	R Cet	M	*silicate B*	SE6
RW And	M	*broad+sil*	SE3	RU Cap	M	*silicate B*	SE8
RX Boo	SR	*broad+sil*	SE3t	S CrB	M	*silicate B*	SE5
RZ Cyg	SR	*broad+sil*	SE3t	U Aur	M	*silicate B*	SE4
UW Cep	M	*broad+sil*	SE3	V1111 Oph	M	*silicate B*	SE5
V462 Cyg	M	*broad+sil*	SE1	V342 Sgr	M	*silicate B*	SE6
W Aqr	M	*broad+sil*	SE3	Z Cyg	M	*silicate B*	SE8
Y Cas	M	*broad+sil*	SE3	Z Pup	M	*silicate B*	SE6
Z Cas	M	*broad+sil*	SE1	CU Cep	SR	*silicate A*	SE6
SV Peg	SR	*broad+sil*	SE3t	RU Cyg	SR	*silicate A*	SE5
AZ Mon	M	*broad+sil*	SE3t	U Her	M	*silicate A*	SE4
				UU Peg	M	*silicate A*	SE5
				X Ori	M	*silicate A*	SE4
				o Cet	M	*silicate A*	SE8

There are three sources (AZ Mon, UW Cep and V462 Cyg) which show slight perturbations at $12.5 - 13$ μm, however it is unclear whether these sources exhibit the feature or not. Therefore these sources have been classified as not showing the feature. Furthermore, in the other spectral feature groups, where the $12.5 - 13.0$ μm feature is less common, we find the same situation: those stars with the feature are non-Mira semi-regular variables and those stars without the feature are Miras. As discussed earlier, Sloan et al. (1996) found that $75-90\%$ of the SR variables in their sample exhibited the feature, while it was seen in only $20-25\%$ of their Mira spectra. This is similar to the results of Begemann et al. (1997), who found that 30% of the Miras in their sample exhibited the $12.5 - 13.0$ μm feature. The smaller size of our sample may explain why we do not find any $12.5 - 13.0$ μm feature amongst the Mira spectra. However, the result still stands that the major difference between stars with or without the $12.5 - 13.0$ μm feature is the variability type. We therefore need to ask the question: why is this feature more visible in SR spectra than in Mira spectra? Is it that there is a dust species that forms around SRs but not around Miras? Or is it that we are seeing high temperature refractory grains in SRs which become coated with other material around Miras? How would this explain the appearance of this feature in the spectrum of the supergiant S Per?

3.1. Miras vs. Semiregular variables

Since we have found a difference in the dust features for Miras and semiregular variables, it seems appropriate to discuss the differences between types of red variables. The basic categories are: Miras, which have regular pulsation with large amplitude ($V \geq 2.5$ mag) and periods longer than 60 days; semiregular (SR) variables, which have less regular pulsation and smaller amplitudes ($V \leq 2.5$ mag); and irregular (L) variables. Furthermore, the SRs can be split into four subgroups; SRa, which have relatively regular periods; SRb with more irregular periods; SRc, which are more luminous and associated with supergiants; and SRd which are warmer as defined by their colours or spectral types. However, the differences and similarities between these groups and their relationships to one another

Table 6. Comparing classifications - Supergiant silicate features

Source	Variability Type	Our Class	SP98 Class
AH Sco	SRc	Sil1	SE5t
KW Sgr	SRc	Sil1	SE6
BU Per	SRc	Sil2	SE7
ST Cep	Lc	Sil2	SE7
V358 Cas	Lc	Sil2	SE6
V540 Sgr	Lc	Sil2	SE6
XX Per	SRc	Sil2	SE7
KY Cyg	Lc	Sil3	SE5
NR Vul	Lc	Sil3	SE4
RS Per	SRc	Sil3	SE5t
SU Per	SRc	Sil3	SE4
UW Aql	Lc	Sil3	SE5
S Per	SRc	Sil4	SE4
UY Sct	SRc	Sil4	SE4

Table 7. AGB stars in the *broad+silicate* group with and without the ∼13 μm feature

with ∼13 μm	without ∼13 μm	variable type
BX Eri		SR
RX Boo		SR
RZ Cyg		SR
SAO 37673		SR
SV Peg		SR
	AZ Mon*	Mira
	UW Cep*	Mira
	V462 Cyg*	Mira
	RR Per	Mira
	RW And	Mira
	UW Cep	Mira
	W Aqr	Mira
	Y Cas	Mira
	Z Cas	Mira

* These spectra may exhibit the feature very weakly. However it is so weak that we feel it is best to class these spectra as *not* showing the 13 μm feature.

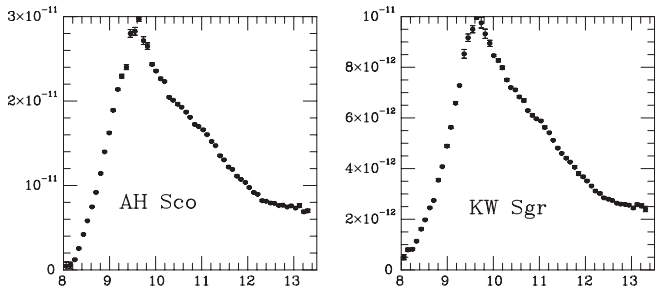

Fig. 11. Continuum-subtracted supergiant spectra classed as showing group 1 *silicate* features. x-axis is wavelength in μm. y-axis is flux in W m^{-2} μm^{-1}

have caused some disagreement in recent years and therefore require further discussion.

It has been suggested in the past that SRs were less evolved than Miras (e.g. Feast & Whitelock 1987), however, given that apart from the 12.5 − 13.0 μm feature, the observed mid-IR spectral features are basically identical for the SR variables and Miras and cover the full range of classifications, this is apparently not reflected in the state of evolution of the dust. Kerschbaum & Hron (1992) also suggested that the SRs and Miras form a continuous sequence, with the SRs the progenitors of the Miras. Furthermore, it has recently been suggested that evolution from SR to Mira is unlikely to be monotonic and that stars may alternate between being Miras and SRs (P. Whitelock, *pers. comm.*; Kerschbaum & Hron 1992). The Miras and SRs have also been found to have separate period-luminosity relations (Whitelock 1986), but whether the separation of these two relations is due to differences in pulsation or stellar structure is unknown (Bedding & Zijlstra 1998). Habing (1996) has suggested that a combination of dust shell structure and mass-loss rate evidence for SRs and Miras implies that Miras are in fact the progenitors of the SR variables. Add this to the uncertainties raised over whether SRs are indeed a separate class to the Miras (Kerschbaum & Hron 1992), and we have a very confused picture.

Mattei et al. (1997) re-investigated the differences between Miras and semiregular variables and found that the groups were indeed distinct from one another based on an examination of the amplitudes of variability and their stabilities. Miras have much more stable amplitudes, while the amplitudes of SRs are much more variable. Furthermore, they were able to divide the SRs into two subgroups based on the amplitude of pulsation and the multiperiodicity. These groups are basically SRa and SRb. Thus, we have evidence that the red variables can be classified into discrete groups rather than a continuous sequence, although whether one variability type is the progenitor of another is still unclear.

Hron et al. (1997) examined dust features in the IRAS-LRS spectra of Mira and SR variables and found a difference between these two stellar types. While they suggested that the Miras are just an extension of the SRs with lower effective temperature, they also found that both Miras and SRs exhibit the full range of mid-IR emission features, from *broad* to the classic, narrow 9.7 μm feature. Furthermore, they found an intriguing difference between these variability types. The Mira spectra behave as we would expect if the sequence from broad to narrow silicate feature is indeed evolutionary, with the optical depth increasing as the feature narrows (i.e. more dust = more evolved dust). However, the SRs showed no such trend and in fact, based on radiative transfer modeling, tended to have more optically thin dust shells for the narrower features (Ivezic & Elitzur 1995). Furthermore, Ivezic & Knapp (1998) found that there was a link

between mass-loss rate and variability type for AGB stars. They found that, while Miras could be fit by "standard" steady-state radiatively driven models, with inner dust-envelope radii defined by the typical condensation temperature (800 − 1000 K), their models required SRs to have a much lower condensation temperature of ∼300 − 400 K. They interpret this as a decrease in the mass-loss, which equates to a less dense dust shell, in agreement with Hron et al. (1997). This is evidence that the SRs should be treated as a distinct group from the Miras, at least as far as dust formation is concerned.

As mentioned above, it has also been suggested that the transition between Miras and SRs is not a single event and happens many times (e.g. Kerschbaum & Hron 1992). A star may have regular, strong, large amplitude pulsations for a time and then have weaker, more irregular pulsation and then go back to strong, regular pulsation as the thermal pulses of the star disrupt the stellar structure. Therefore, it is possible that the 12.5 − 13.0 μm feature needs to be explained in terms of a dust species that can only form in the environment of an SR, and is either rapidly destroyed or over-coated by a lower condensation temperature material in the environment of the Miras or has been ejected by the stellar wind prior to the Mira phase. The small percentage of Miras found by Sloan et al. (1996) to exhibit the 12.5 − 13.0 μm feature might be explained in terms of stars that have recently changed from SR to Mira and have not yet destroyed/lost their complement of the carrier of the 12.5 − 13.0 μm feature.

As discussed in the introduction, Justtanont et al. (1998) found a correlation between CO_2 emission lines and the 12.5 − 13.0 μm feature. This was taken as evidence that both the CO_2 and the carrier of the 12.5 − 13.0 μm feature were formed in warm gas layers close to stars with low mass-loss rates, in particular the lower density dust shells around SRs. Since the strengths of the 12.5 − 13.0 μm and CO_2 emissions are correlated and higher mass-loss rates appear to preclude formation/excitation of the CO_2 lines, higher mass-loss rates may also inhibit the formation of the 12.5 − 13.0 μm carrier.

3.2. Which minerals?

Previously, the 12.5 − 13.0 μm feature has been identified with Al_2O_3 grains (Hackwell 1972; Vardya et al. 1986; Onaka et al. 1989; LML90, Glaccum 1995), however there are problems with this attribution. Al_2O_3, or alumina is found in several different forms. Only one form occurs naturally on the earth: corundum or α-Al_2O_3. This has rhombohedral crystal structure and is known by various other names including ruby or sapphire depending on the trace impurities (Deer et al. 1966, hereafter DHZ). There are known synthetic polytypes: β-Al_2O_3, which has hexagonal crystal structure; and γ-Al_2O_3 which is cubic. However both these forms convert to corundum on heating (DHZ). It is also possible to make amorphous samples (e.g. Begemann et al. 1997). Some condensation models (Salpeter 1974; Sedlmayr 1990; Tielens 1990; Kozasa & Sogawa 1997, 1998) suggest that Al_2O_3 should be the first dust type to condense around O-rich stars. According to some previous research (e.g. Vardya et al. 1986; Onaka et al. 1989; Tielens 1990; Kozasa & Sogawa 1997, 1998), Al_2O_3 then forms a nucleation seed on which the silicates can form a mantle. Alternatively, Nuth & Hecht (1990) and Stencel et al. (1990) suggested that the condensate is a "chaotic silicate" in which, initially, the emission from Al-O bonds dominates the spectra, but is then overwhelmed by emission from the more abundant Si-O bonds. Both sets of authors agreed that the 12.5 − 13.0 μm band seen in the spectra of oxygen-rich stars can be attributed to Al-O bonds and that it signifies the presence of some form of aluminium oxide. Moreover, Al_2O_3 grains found in meteorites (Nittler et al. 1994a,b, 1997; Huss et al. 1995) have isotopic signatures which suggest they were formed around oxygen-rich AGB stars. However, the abundance of such AGB star Al_2O_3 grains is very low (< 1 ppm; cf. 6 ppm for presolar SiC and 400 ppm for presolar diamond). Furthermore, the polytype (i.e. the crystal structure) of these presolar Al_2O_3 grains is as yet unknown (L. Nittler, *pers. comm.*) so that no information on the exact spectral features we should expect has yet been gleaned from these meteoritic grains.

Begemann et al. (1997) studied the laboratory spectra of various forms of aluminium oxide, both crystalline and amorphous, with a view to identifying more clearly the 12.5 − 13.0 μm feature seen in IRAS-LRS spectra. They found that amorphous aluminium oxide could not account for the observations and that, while the α- crystalline form of Al_2O_3 could account for the 12.5 − 13.0 μm feature, a second feature seen at 21 μm in laboratory spectra of this material was not observed in astronomical spectra. Indeed, the two spectra of Al_2O_3 shown in Fig. 18 have peak positions in the 11.5 − 12.0 μm range, rather than at 12.5 − 13.0 μm. Begemann et al. (1997) suggested that the 12.5 − 13.0 μm feature may come from a form of silicate rather than from aluminium oxide. Furthermore, we may note that if the 12.5 − 13.0 μm feature was attributable to the first condensate, it would be expected to appear predominantly in the *broad* feature spectra. As stated above, the 12.5 − 13.0 μm feature appears most commonly in our spectra in the *broad+sil* class, and is certainly not ubiquitous. In addition, the appearance of the feature seems to be related to the variability type of the AGB star (i.e. Mira or SR). Given that Al_2O_3 is so important to the theoretical condensation sequence, and that the spectral features of Al_2O_3 do not seem to match the observed astronomical features, it seems doubly unlikely that the 12.5 − 13.0 μm feature is attributable to Al_2O_3.

Kozasa & Sogawa (1997, 1998) proposed grains consisting of Al_2O_3 cores and silicate mantles for the carrier

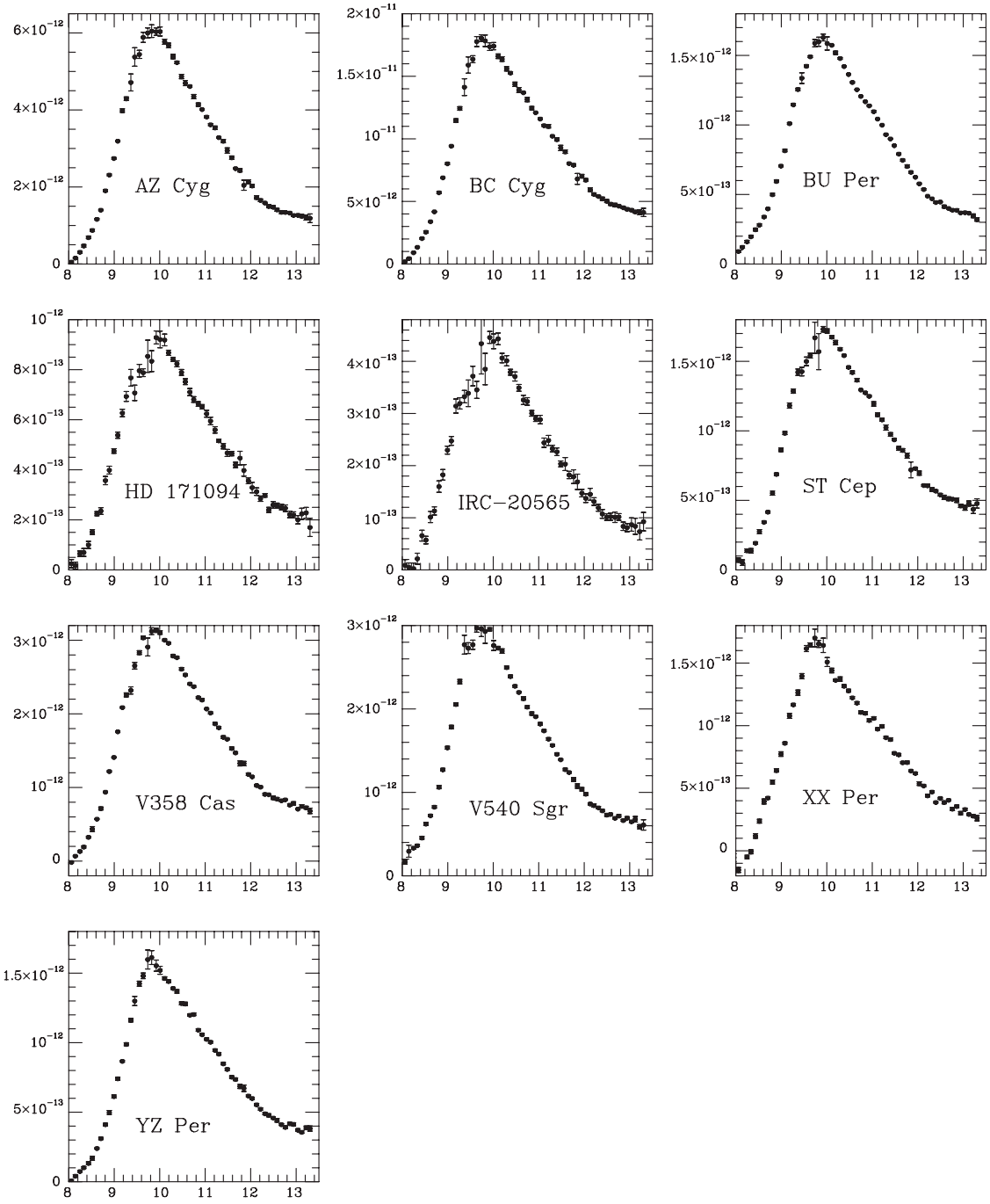

Fig. 12. Continuum-subtracted supergiant spectra classed as showing group 2 *silicate* features. x-axis is wavelength in μm. y-axis is flux in W m^{-2} μm^{-1}

of the 12.5 − 13.0 μm feature. However, this was investigated by Posch et al. (1999) who found that: 1) there would have to be a large population of grains of ∼85% Al_2O_3; and 2) there would have to be an even larger number of pure silicate particles to produce anywhere near the correct ratio of 13 μm to 10 μm flux strengths. They, therefore, concluded that such core-mantle grains were unlikely to be the carriers of the 12.5 − 13.0 μm feature.

Another possible carrier for the 12.5 − 13.0 μm feature is spinel, $MgAl_2O_4$, as proposed by Posch et al. (1999) who compared laboratory and calculated spectra of various candidate minerals with ISO-SWS spectra of AGB stars which exhibit the 13 μm feature. Posch et al. argue against Al_2O_3 as the carrier for many of the reasons summarized here, and concluded that the most likely mineral to produce the 13.0 μm feature is spinel ($MgAl_2O_4$).

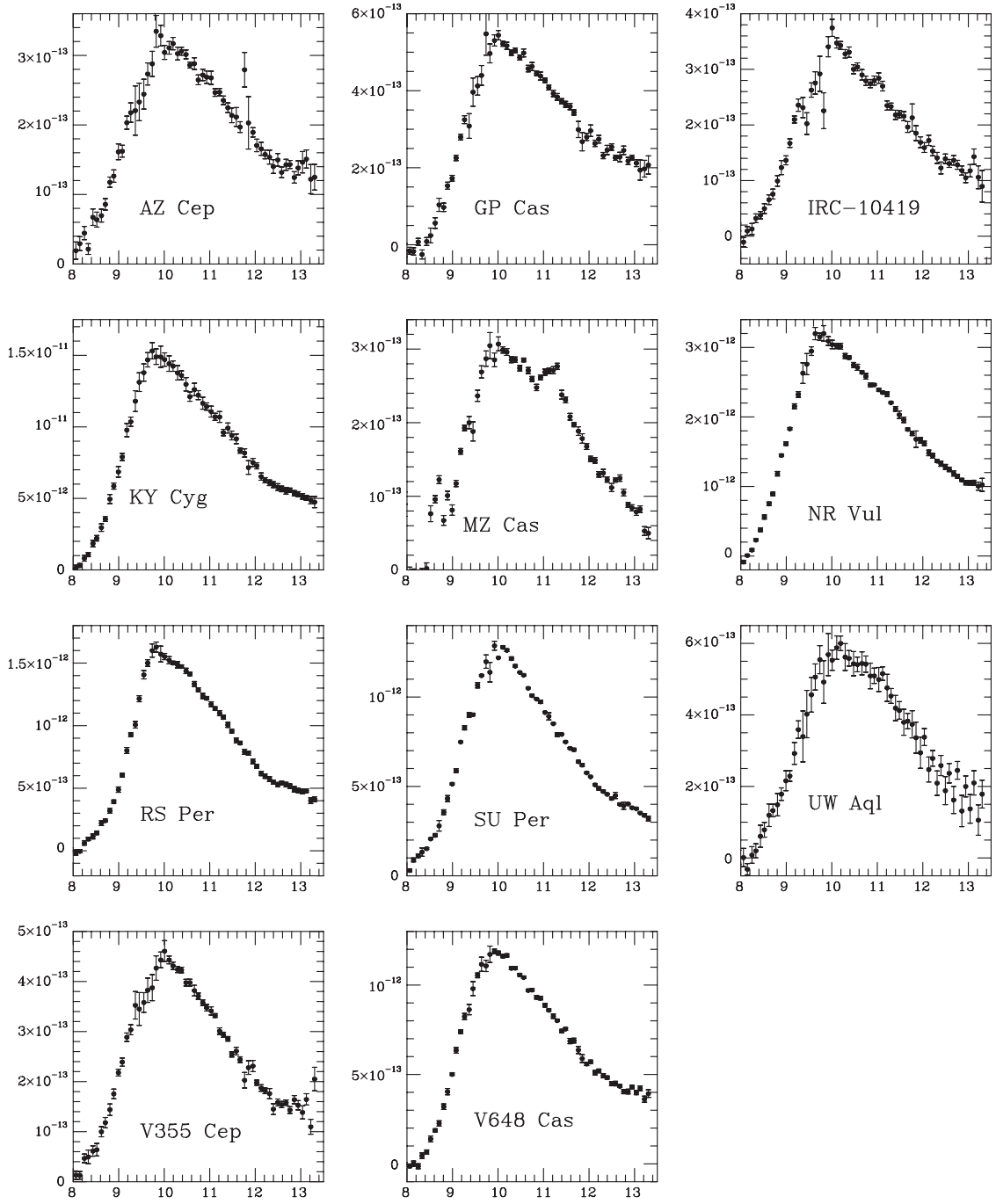

Fig. 13. Continuum-subtracted supergiant spectra classed as showing group 3 *silicate* features. x-axis is wavelength in μm. y-axis is flux in W m^{-2} μm^{-1}

Spinel is a very refractory, cubic mineral which is found naturally on the earth (DHZ). It has also been found as a presolar grain in meteorites (Nittler et al. 1994a, 1994b, 1997). However, this attribution is compromised by problems with the spinel optical data. Posch et al. (1999) used optical data from Tropf & Thomas (1991) which is potentially flawed, since the optical constants are based on a compilation of different data mostly from synthetic samples. Tropf & Thomas noted that where more than one data set exists for the same wavelength region, the measurements do not necessarily match up. Following Andreozzi et al. (2000), it has become clear that, for spinel in particular, the precise level of order/disorder of the crystal structure can have a large effect on the optical

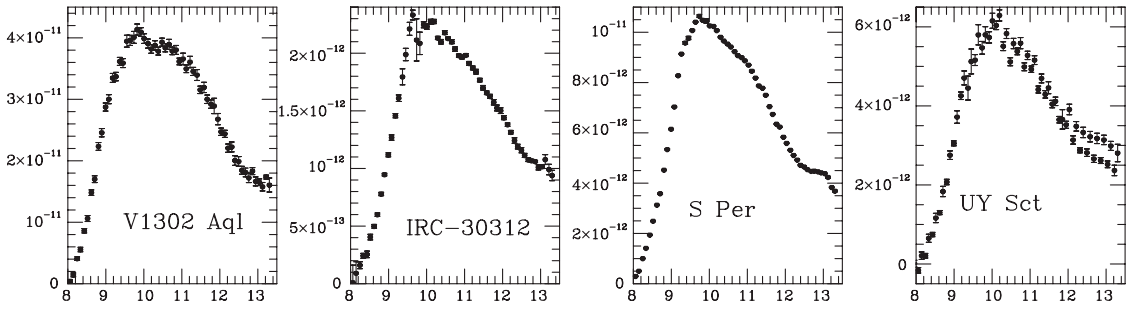

Fig. 14. Continuum-subtracted supergiant spectra classed as showing group 4 *silicate* features. x-axis is wavelength in μm. y-axis is flux in W m^{-2} μm^{-1}

properties. The Mg/Al order varies among the synthetic samples and affects the IR spectra in both the width and number of peaks. Thus, the optical constants n and k depend on Mg/Al order, which in turn may depend on the formation temperature. This renders compilations of data for spinel, such as that of Tropf & Thomas (1991), moot since such compilations do not take into account the issue of the differing amounts of order/disorder in the differing samples. Therefore the positions of the spectral features derived by Posch et al. (1999) from the Tropf & Thomas data are unlikely to be valid for any one sample of spinel. Previous studies of crystalline spinel have found peaks at wavelengths longwards of 13.5 μm (e.g. Chopelas & Hofmeister 1991; Hafner 1961; Preudhomme & Tarte 1971). Indeed, it was these previously published spectra which prompted Speck (1998) to ignore spinel in her discussion of mid-IR dust features because it did not appear to have any features in the $7.5 - 13.5$ μm window and would therefore not be a candidate for the 13 μm feature. Clearly the issue of spinel and its intriguing IR spectral behaviour requires more investigation, but that is beyond the scope of the current work.

Our results support the findings of Begemann et al. (1997) by associating the 13 μm feature with silicates. This observed feature appears to be best explained in terms of some form of silicate (Begemann et al. 1997) or SiO_2 (silica; Speck 1998). Both copper ($Cu(II)SiO_4$) and zinc ($ZnSiO_4$) silicates exhibit this spectral feature (Speck 1998), but it is not seen in the spectra of the more commonly expected magnesium, calcium or aluminium pyroxene or olivine silicates. Copper and zinc are not abundant enough to form observable quantities of such silicates. The silicates of magnesium, calcium and aluminium which are expected to form in these circumstellar environments are pyroxenes (i.e. chain silicates) and olivines (i.e. individual units of silicate tetrahedra; see Speck 1998 for a discussion of silicate structures). Silicon dioxide, on the other hand, forms a "fully polymerized" crystal lattice. Intermediate between SiO_2 and the pyroxenes are the sheet silicates. From a spectral feature point of view, there is a progression from SiO_2, with a relatively strong 13 μm feature (Fig. 18d), through the sheet silicates, where the 13 μm feature diminishes, to pyroxenes which generally do not show this feature. Although silica is chemically an oxide, the structures and properties of the silica minerals are more closely allied to those of silicates. SiO_2 can be either crystalline or amorphous. There are three main polytypes for crystalline SiO_2: quartz, tridymite and cristobalite. These forms may be seen as a progression in the temperature of formation (DHZ). Silica can also exist in amorphous forms such as lechaterlierite, obsidian and silica glass. The different forms of silica and their stable temperatures are discussed in more detail by Speck (1998). Furthermore, the available atomic abundances are perfectly acceptable for the formation of observable quantities of SiO_2. Therefore, it is plausible on abundance grounds that silicon dioxide or a sheet silicate is responsible for the 13 μm feature, so an SiO_2 origin for the 13 μm feature deserves further exploration.

4. Dust condensation sequence

The dust condensation sequence in O-rich circumstellar regions is expected to go as follows (Tielens 1990):

$$
\begin{array}{cc}
Al_2O_3, \text{Alumina} & \\
\Downarrow & \\
Ca_2Al_2SiO_7, \text{Augite} & \\
\Downarrow & \\
CaMgSi_2O_6, \text{Diopside} & Mg_2SiO_4, \text{Forsterite} \\
\Downarrow & \Downarrow \\
MgAl_2O_4, \text{Spinel} & MgSiO_3, \text{Enstatite} \\
\Downarrow & \Downarrow \\
CaAl_2Si_2O_8, \text{Anorthite} & (Mg, Fe)_2SiO_4, \text{Olivine}
\end{array}
$$

According to condensation thermodynamics, the silicate condensation sequence starts with the nucleation of alumina (Al_2O_3) from the circumstellar gas at about 1760 K. The first silicate is expected to form by a gas-solid reaction with alumina, to form $Ca_2Al_2SiO_7$. As the temperature drops, further gas-dust reactions occur so that Mg substitutes for Al to form $CaMgSi_2O_6$. The aluminium released and the remaining alumina are converted to spinel ($MgAl_2O_4$). As further cooling occurs the $CaMgSi_2O_6$

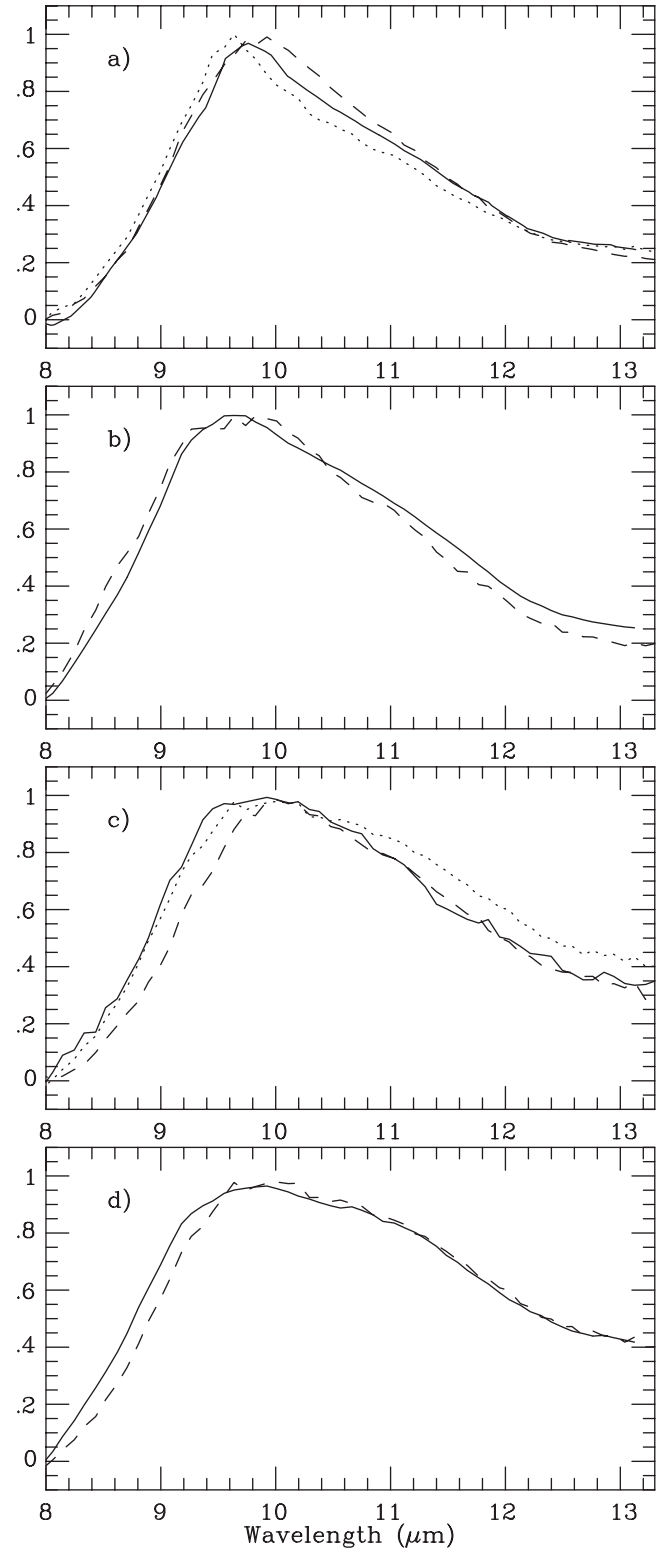

Fig. 15. Comparison of the silicate features of AGB stars and supergiants. **a)** AGB silicate group A (solid line) vs. supergiant silicate groups 1 (dotted line) and 2 (dashed line); **b)** AGB silicate group B (solid line) vs. unclassified supergiant U Lac (dashed line); **c)** AGB silicate group C vs. supergiant silicate groups 3 (dashed line) and 4 (dotted line); **d)** AGB silicate group D vs. supergiant silicate group 4 (dashed line)

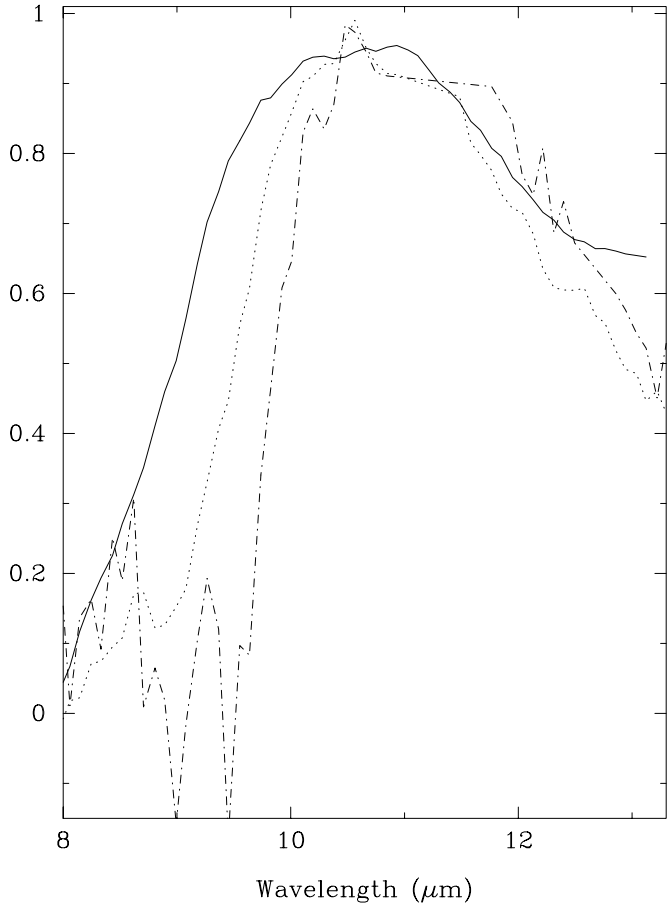

Fig. 16. Comparison of the average *broad* features for AGB stars (solid line) and supergiants (dotted and dashed lines)

and the spinel form a solid-solid reaction, producing the feldspar anorthite ($CaAl_2Si_2O_8$). At even lower temperatures ($\sim$ 1440 K) forsterite (Mg_2SiO_4) starts to condense out. Forsterite continues to form until the temperature has dropped to $\sim$ 1350 K when it reacts with gaseous SiO to produce enstatite ($MgSiO_3$). Finally, at $\sim$ 1100 K reactions with gaseous iron will convert some enstatite into fayalite (Fe_2SiO_4) and forsterite. Kinetics also plays an important role in determining which silicates form in the outflows of AGB stars. Depending on the density structure of the circumstellar region the condensation sequence will cease at different points. Thus, if the density drops rapidly with distance from the star, the only dust expected to form will be various high temperature oxides (e.g. Al_2O_3, $CaTiO_3$, ZrO_2), which will form very close to the star. If the densities are a little higher further out in the circumstellar shell gas-grain reactions can take place, allowing the formation of calcium-aluminium silicates. If the density is high enough a little further out still magnesium silicates may form as rims on the Ca-Al silicates. For magnesium silicates to nucleate, there need to be very high densities a long way out, which is highly unlikely. Feldspars, such as anorthite ($CaAl_2Si_2O_8$) are not expected to form, as the solid-solid reaction requires

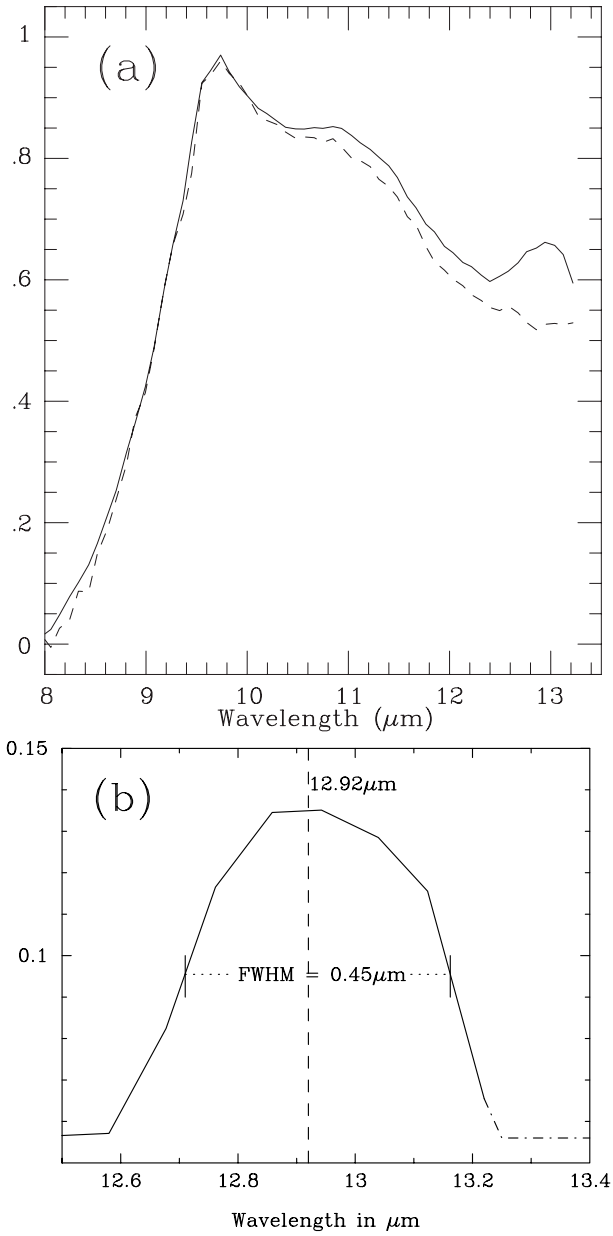

Fig. 17. The 12.5 − 13.0 μm feature. **a)** the mean spectra for stars in the *broad+silicate* group, with (solid line) and without (dashed line) the ∼13 μm feature; **b)** the isolated ∼13 μm feature. This was achieved by subtracting the mean spectrum without the ∼13 μm feature from the mean spectrum with the ∼13 μm feature. The dashed line shows the peak position of the feature. FWHM = full width at half maximum

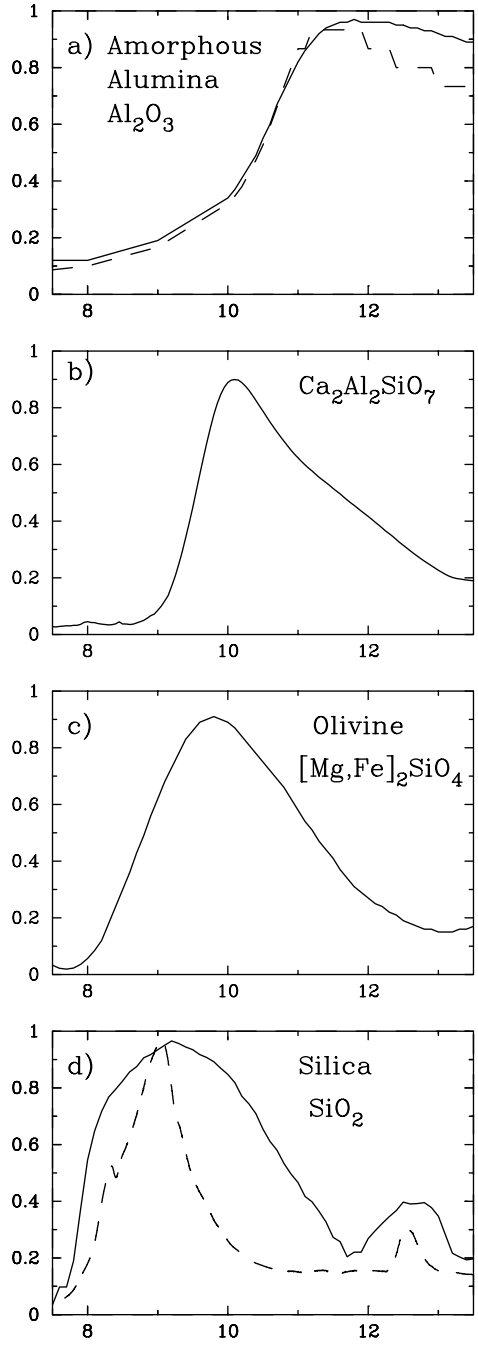

Fig. 18. The laboratory spectra of some minerals in the predicted condensation sequence. In **a)** two spectra are shown for amorphous alumina, where the solid line represents a porous sample and the dashed line is a compact sample. These spectra both come from the Jena optical constants database (http://www.astro.uni-jena.de/Group/Subgroups/Labor/Labor/odata.html), as do the spectra in **b)** and **c)**. In **d)**, two polytypes of SiO_2 are shown. The solid line is a form of amorphous silica (from Nyquist 1971) and the dashed line is one of the crystalline polytypes, tridymite (Hofmeister et al. 1992). The x-axis is wavelength in μm, the y-axis is normalized extinction

unrealistically high densities. Finally, Fe can only be incorporated into Mg-silicates if, initially, most of the iron is in gaseous form (rather than solid, metal form) and if the density is high enough at large distances from the star where fayalite (Fe_2SiO_4) can survive. Figure 18 shows the laboratory spectra of major minerals that are expected to form, together with that of SiO_2 which is a likely to be a step in the formation of silicates.

Another possible sequence of condensation mentioned by SP98 involves chemistry determined by the C/O ratio. In this case, less evolved stars with low C/O ratios would exhibit silicate features while somewhat more evolved stars, with C/O ratios closer to unity, could have spectra dominated by Al_2O_3. According to the standard scenario (e.g. Salpeter 1974), stars with low C/O ratios ($\ll$1), have an abundance of oxygen atoms to form dust and therefore we should see strong silicate features. However, in stars with higher C/O ratios (but still less than unity) less oxygen would be available and therefore aluminium oxide features could dominate because aluminium is more oxidizing than magnesium and so uses up the available oxygen first (see SP98 for details).

5. Discussion

The first obvious manifestation of the differences between AGB and supergiant spectra is the difference in their *broad* features. However, the various "silicate" features are basically identical for both AGB stars and supergiants (see Fig. 15). Therefore, assuming that the observed spectral features represent evolution of the dust from the most refractory species, responsible for the broad features, to magnesium-rich silicates, it is clear that the AGB star condensation sequence is different from that of supergiants but both condensation sequences eventually leading to similar dust types, i.e. magnesium-rich silicates. The suggested evolutionary paths for the dust around O-rich AGB stars and supergiants are shown in Table 8. To explain these we need to have distinct differences between the dust-forming regions of AGB stars and supergiants in terms of elemental abundances, oxidation properties, temperatures or densities of the dust-forming atmospheres.

The difference between the broad features exhibited by O-rich AGB stars and supergiants implies a different pathway to the magnesium-rich silicates. The short-wavelength rise of the supergiant *broad* feature may be indicative of calcium-aluminium-rich silicates, e.g. $Ca_2Al_2SiO_7$, which match this part of the spectrum well (Fig. 19a). However, thus far no Ca-Al-rich silicate spectrum has a broad enough feature to account for the entire *broad* band. A second spectral feature peaking at about $11.5 - 12.0$ μm and extending to beyond the 13.5 μm limit of our spectra is needed to account for the long wavelength part of the *broad* feature. This feature (but not the $12.5 - 13.0$ μm feature) could be attributable to alumina (Al_2O_3). Likewise the short wavelength onset of the AGB star *broad* feature may be due to Mg-Fe-rich silicates, but again this does not account for the long wavelength part of the feature. However, the shape of the long wavelength feature needed to complete the broad feature in both the AGB star and supergiant cases is very similar. We have found that this extra feature is best fit using alumina (Al_2O_3), although the exact form of alumina is not identical in each case to account for the flux longwards of $\sim$ 13 μm. Figure 19a shows that the supergiant broad feature can be fit using a combination of Ca-Al-rich silicate ($Ca_2Al_2SiO_7$) and compact amorphous alumina, while the AGB star *broad* feature (Fig. 19b) can be fitted using a combination of olivine ($MgFeSiO_4$) and porous amorphous alumina.

Table 8. The different evolutionary paths of dust around AGB stars and around supergiants

AGB stars	Supergiants
$(Mg, Fe)_2SiO_4$ & Al_2O_3	$Ca_2Al_2SiO_7$ & Al_2O_3
$\Downarrow$	$\Downarrow$
$(Mg, Fe)_2SiO_4$ strengthens	No obvious transition feature
$\Downarrow$	$\Downarrow$
$(Mg, Fe)_2SiO_4$ overwhelms broad feature	$(Mg, Fe)_2SiO_4$ overwhelms broad feature
13 μm feature in some spectra	No 13 μm feature

Therefore the main difference between the supergiant and AGB dust features seems to be that the supergiants have a distinct evolutionary phase in which calcium-aluminium-rich silicate condensation takes place to an extent that is observable, whereas for AGB stars this phase is not seen. The first distinct spectral features to be seen in AGB star spectra can be attributed to a combination of Mg-Fe-rich silicates and alumina. The AGB stars go through a phase in which the Mg-Fe-rich silicate feature strengthens and eventually overwhelms the alumina feature. The supergiant spectra exhibit either Ca-Al silicate and alumina features or strong Mg-Fe silicate features. No transitional states have been observed.

The $12.5 - 13.0$ μm feature seen in the spectra of some AGB stars is almost completely absent from the supergiant spectra, appearing only in the spectrum of S Per, a supergiant with a particularly thin dust shell similar to that of SRs (see Sect. 2.3.2; Richards 1997; Richards et al. 1999). Therefore, whatever dust species is responsible for this feature is not included in the usual condensation sequence for supergiants. As discussed in Sect. 3, the $12.5 - 13.0$ μm feature is predominantly seen in the spectra of semiregular variables, so there must also be a difference between dust-forming properties of Miras and semiregular variables. We suggest that this feature is not due to Al_2O_3, $MgAl_2O_4$, or core-mantle alumina-silicate grains, as has previously been proposed (e.g. Vardya et al. 1986; Posch et al. 1999; Kozasa & Sogawa 1997, 1998

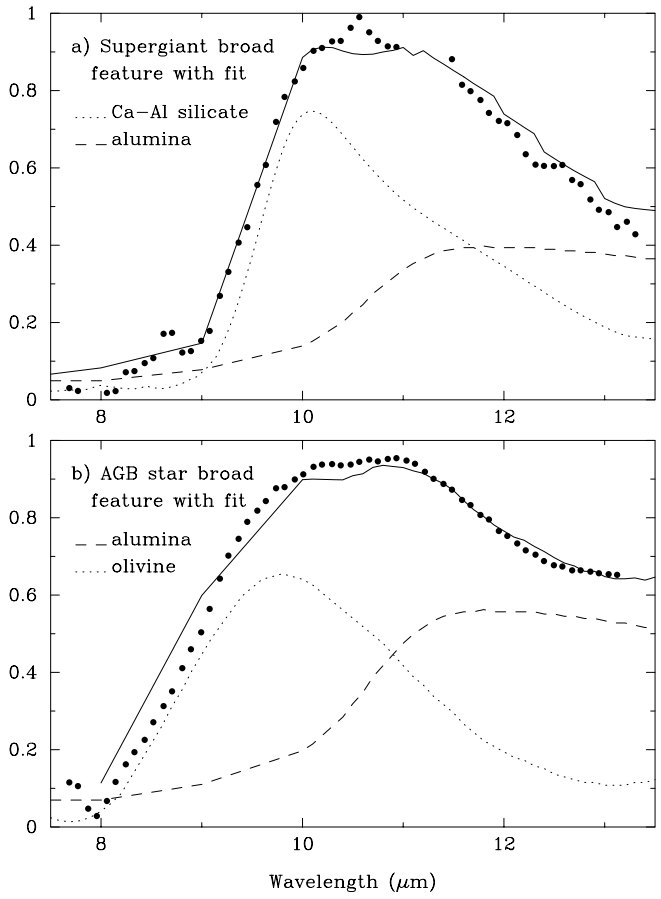

Fig. 19. Fits to *broad* features. **a)** The supergiant *broad* feature is fit by $Ca_2Al_2SiO_7$ (dotted line) and compact amorphous Al_2O_3 (dashed line). **b)** The AGB star *broad* feature is fit by $MgFeSiO_4$ (dotted line) and porous amorphous Al_2O_3 (dashed line)

respectively), but rather that it may be associated with silicon dioxide (see Morioka et al. 1998; Speck 1998), which also accounts for the 9.25 μm peak seen in the spectra of some AGB stars with strong silicate features (see Speck 1998). Another possible carrier may by highly polymerized silicates which bear more structural resemblance to SiO_2 than to isolated silicates like olivine.

The difference between the chemistries of Miras, semiregular variables and supergiants needs to be addressed. There are two proposed *dust sequences* (for want of a better term): the classic condensation sequence discussed in Sect. 4 (see also Tielens 1990); and the new chemical evolution sequence based on C/O ratios (SP98). The SP98 model was constructed using a dataset that had no supergiant spectra exhibiting the *broad* feature. With this supergiant *broad* feature included, we need to re-examine the possibilities.

AGB stars experience the so-called "third dredge-up" which brings the products of the helium-burning shell to the surface of the star (see e.g. Iben & Renzini 1981). In particular, this process enriches the atmospheres of these stars with ^{12}C. With successive dredge-ups the atmospheres of AGB stars get progressively more carbon-rich. Therefore oxygen-rich AGB stars can have carbon-to-oxygen ratios (C/O) ranging from cosmic, ∼0.4, to approximately unity. Supergiants, on the other hand, are not expected to experience a "third dredge-up" and are therefore expected to remain oxygen-rich, with approximately cosmic C/O. Furthermore, Sylvester et al. (1994) found UIR bands in the spectra of some M-supergiants. They suggested that UV photodissociation of CO molecules provided the free carbon atoms required to form the organic materials responsible for the UIR bands. Obviously, this dissociation mechanism would also release extra oxygen atoms, and if the carbon atoms become trapped in organic molecules, this could lead to an even more oxygen-rich environment (C/O $<$ 0.4). Therefore, supergiants exhibiting the UIR bands could have even more oxygen available for dust formation and, following the SP98 scheme, we might expect these stars to exhibit the "classic" strong silicate spectral feature, since they should have more than enough oxygen to make substantial amounts of Mg-silicates. However, many of the supergiants with UIR bands exhibit "broad" spectral features. These supergiant "broad" spectral features are alone enough to call into question a condensation mechanism based on the amount of available oxygen, since the C/O ratio for supergiants is always low. Combining this with the UIR band evidence, it seems unlikely that the type of dust forming around these stars is determined solely by the amount of oxygen available.

Contrary to SP98, we have found that the "broad" feature in AGB star spectra cannot solely be attributed to Al_2O_3. The feature appears to be due to a combination of Al_2O_3 and "classic" silicate (e.g. amorphous olivine). A fit to the average "broad" feature spectrum using Al_2O_3 and amorphous olivine is shown in Fig. 19b. This does not contradict the SP98 dust evolution scheme, but implies that oxygen availability is never so low as to preclude some silicate formation. It does, however, cause a problem for the supergiant sequence. The SP98 scheme cannot account for the formation of Ca-Al-rich silicates rather than Mg-Fe-rich silicates in the very oxygen-rich supergiant environments, where there should be more than enough oxygen to form the "classic" silicates.

It is clear that the C/O ratio is an important factor in determining which dust species will form around which stars, however, other factors (e.g. dust shell temperature and density) are also important and need to be taken into account. In trying to accommodate as much of the available information, and previous interpretations, as possible, the current work suggests the following: the type of dust species formed around a given star is controlled by the C/O ratio and by the density and temperature of the dust-forming region, but that one of these factors will

dominate, depending on the exact balance between the C/O ratio, the density and the temperature. The work of Hron et al. (1997) suggested that the classical condensation sequence is valid for Miras, since they found that the "classic" narrow silicate feature is associated with the most optically thick dust shells (i.e. more dust = more evolved dust). This is not the case for the semiregular variables. In fact, for these the optical depth is lowest for the narrowest silicate features and is higher for the broader features (Ivezic & Elitzur 1995). However, the most optically thick SR dust shells are only as optically thick as the most optically thin Mira dust shells. This may be the key to the problem. In the case of the Miras, with relatively high optical depths, and therefore relatively high density dust shells, it is the density of the dust shells that controls the dust formation, and these environments undergo dust formation which follows the classic condensation sequence. For Miras the evolutionary stage of the dust reflects the evolutionary stage of the star (i.e. Miras with broad features are less evolved than those with the "classic" silicate features). In the case of SRs, with much less dense shells, it is the C/O ratio that controls the dust formation and therefore the dust "evolution" follows the opposite path to the classic condensation sequence, as suggested by SP98. This fits with the findings of Hron et al. (1997). In the case of the SRs, the stars with the "classic" silicate feature are less evolved, with less dense dust and more free oxygen, while the "broad" feature is associated with more evolved SRs, which have denser dust shells and fewer available oxygen atoms.

We now return to the enigmatic 13 μm feature. This feature appears to be associated with SR variables and therefore with less dense dust-forming regions. Following the above argument, this in turn implies that species formation is dominated by the C/O ratio. However, it is not clear that the 13 μm feature is associated with any other dust feature. While Begemann et al. (1997) found a close correlation between this feature and the classic silicate feature, both Sloan et al. (1996) and the current work found that the 13 μm feature is not particularly associated with any of the other dust features – appearing in examples from all classes and implying that the 13 μm feature is not associated with the evolutionary stages of the dust around SRs, or the prevailing C/O ratio. Furthermore, it is rarely found in supergiant or Mira spectra. It has been suggested that the 13 μm feature is carried by silicon dioxide (SiO_2; Speck 1998). However, some objections to this attribution have been raised. Firstly, there is the exact position of the feature at $\sim$12.9 μm. Posch et al. (1999) state that the feature in amorphous SiO_2 peaks at 12.3 μm, which is too far removed from the observed feature. However, infrared spectra of different polytypes of SiO_2 presented by Speck (1998) show that the "13 μm" feature peak position varies from one polytype to another from $\sim$12.5 μm to $\sim$12.8 μm, with the feature width (FWHM) varying from 0.33 to 0.73 μm. While this is still not identical to the observed feature, it is much closer than any other suggested carrier. Second, there are other spectral features in the infrared spectrum of SiO_2 which need to be accounted for. As shown in Fig. 18, SiO_2 has two features in the $7-14$ μm range relevant to our observed spectra, the $12.5-13$ μm feature and a stronger 9.2 μm feature. There is also a feature at $\sim$20 μm outside the range of our observations. The relative strength of the 13 μm feature to the other features depends on the polytype (i.e. crystal structure; see Speck 1998), the level of disorder of the crystal structure, and the relative optical depths (Hofmeister et al. 2000). While the 13 μm feature is usually weaker than the 9.2 μm feature, optical depth effects can hugely increase the relative strength of the 13 μm feature (see Hofmeister et al. 2000). The observed 13 μm feature is never found in isolation – there is always some contribution in the $8-10$ μm region, probably from Si-O bond stretching in amorphous forsterite/enstatite. It is possible to bury the 9.2 μm feature in this general Si-O stretch region, so that the only evidence for SiO_2 above the general silicate contributions to the spectra is the 13 μm feature. In fact, there is some evidence for an emerging 9.2 μm feature, over and above the "classic" 9.7 μm silicate feature, which may be attributable to SiO_2 (Speck 1998). It is possible that the $\sim$20 μm SiO_2 feature could be buried in the amorphous silicate Si-O bending feature nearby, but this cannot be assessed with the current observations. However, it was noted by LML90 and Goebel et al. (1989) that the 13 μm feature seen in IRAS spectra was often associated with an unidentified feature at about $19-20$ μm, and this may be the other SiO_2 spectral feature. Another objection raised to SiO_2 is that equilibrium calculations have shown that it is not expected to form around AGB stars (Lodders & Fegley 1999). Any SiO_2 that does form is expected to be rapidly converted to forsterite and then enstatite. The key point, however, is that objection requires that equilibrium is reached. In order to form forsterite and enstatite, the condensation sequence is likely to go through SiO_2 formation. Current thinking has been that SiO_2 forms at most only a minor constituent of the dust, but this is based on the absence of observed features near 9.2 and 12.5 μm and a shoulder near 8.4 μm (J. Nuth, *pers. comm*), which, as stated above, may be buried in the strong Si-O stretching feature. If equilibrium is not reached, we would expect there to be some residual SiO_2 in these regions. In Miras, the denser dust shells are more likely to reach equilibrium than the less dense SR dust shells because each atom/molecule in a denser environment has more chance of interacting with another atom/molecule. This might explain the formation of a disequilibrium product (SiO_2) in the less dense SR dust shells and not in the denser Mira dust shells.

In Sect. 3, we discussed the difference between SRs and Miras. It is not clear whether SRs are the progenitors of Miras or vice versa, whether these stars go through successive SR and Mira phases, or whether they are

completely separate objects. However, assuming that they are related and that SRs may evolve into Miras and then back into SRs, how can we account for the appearance of a species in the dust-forming region of one of these variability types and not in the other? The easiest explanation is to assume that the dust around SRs, which we assume includes some SiO_2 or highly polymerized silicate, is ejected by the stellar wind prior to the Mira phase and then does not form again until the star returns to the SR phase. Alternatively, the dense dust regions around Miras may cause the SiO_2-rich (parts of) grains to be transformed into olivines and pyroxene as the progression towards equilibrium is enhanced in the denser environment. It is known that the implantation of impurities, such as metal ions, tends to transform SiO_2 and highly polymerized silicates into less polymerized silicates like olivines and pyroxenes (Zachariasen 1932; Hess 1995). The less dense dust forming regions around SRs would allow more of the purer SiO_2/highly polymerized silicate grains to form and survive. All other features in the spectra of Miras and SRs are identical. The fact that SiO_2/highly polymerized silicate is plausible from an abundance point of view and that the disappearance of the species in Mira spectra can be explained makes the attribution of the 13 μm feature to SiO_2 or highly polymerized silicates even more attractive. While laboratory spectra of SiO_2 are commonly available, as discussed above, the position of the $12.5 - 13.0$ μm feature is not ideal. Therefore, laboratory studies of highly polymerized silicates are needed to find a better match to the observed feature.

How do we relate these ideas to the supergiants? Most supergiant spectra do not exhibit the 13 μm feature. They seem to follow a different chemical evolution to either Miras or SRs. While many supergiant spectra show "classic" silicate features identical to those in AGB stars, it is the difference in the broad feature that is the mystery. We have to ask: what differences between supergiants and AGB stars can shed light on this problem? One obvious difference is that some supergiants exhibit UIR emission bands, attributed by Sylvester et al. (1994, 1998) to the presence of chromospheres around such supergiants, whereas AGB stars do not have chromospheres. The presence of a strong UV radiation field in supergiant outflows, as well as dissociating CO and permitting the formation of the carbon-rich UIR-band carriers, may also significantly influence the early dust formation sequence in the remaining oxygen-rich gas once the UIR-band carriers have formed.

Another avenue for future investigation is the relation of asymmetry factors for AGB stars to their dust spectra. It has been suggested that the asymmetry of the light curve of an AGB star is related to its evolutionary stage (Vardya et al. 1986). Unfortunately it appears that useful published data is only available for the light curves of Miras, so that comparison of the light curves of Miras to those of SRs is not currently possible. Other factors to take into account in future work are dust feature strength and profile variations as a function of pulsation cycle phase, as studied by Monnier et al. (1998) and earlier workers, and the secular long-term variation of the observed dust features of some sources that was discovered by Monnier et al. (1999).

Acknowledgements. We would like to thank Icko Iben, Teije de Jong, Katharina Lodders, Larry Nittler, Joe Nuth, Hans Olofsson, Anita Richards, Patricia Whitelock, and Elric Whittington for useful email correspondence/chats. An anonymous reviewer is also thanked for constructive criticism, which was instrumental in significantly improving this paper. AKS would like to dedicate this work to the memory of J. Colin Siddons, physics teacher, mentor and friend, who died in November 1999.

References

Andreozzi G.B., Princivalle F., Skogby H., Della Giusta A., 2000, American Mineralogist (in press)
Aringer B., Höfner S., Wiedemann G., et al., 1999, A&A 342, 799
Bedding T.R., Zijlstra A.A., 1998, ApJ 506, L47
Begemann B., Dorschner J., Henning T., et al., 1997, ApJ 476, 199
Cernicharo J., 1998, Ap&SS 255, 303
Chopelas A., Hofmeister A.M., 1991, Phys. Chem. Min. 18, 279
Cohen M., Davies J.K., 1995, MNRAS 276, 715
Creech-Eakman M.J., Stencel R.E., Williams W.J., Klebe D.I., 1997, ApJ 477, 825
Deer W.A., Howie R.A., Zussman J., 1966, An Introduction to the Rock Forming Minerals. Longman Scientific & Technical: London
Feast M.W., Whitelock P.A., 1987, in Late stages of stellar evolution, p. 33
Gail H.-P., Sedlmayr E., 1998, in Chemistry & Physics of Molecules & Grains in Space, Sarre P. (ed.), Faraday Discussion, No. 109, 303
Gail H.-P., Sedlmayr E., 1999, A&A 347, 594
Gilman R., 1969, ApJ 155, L185
Gillett F.C., Low F.J., Stein W.A., 1968, ApJ 154, 677
Glaccum W., 1995, in From Gas to Stars to Dust, Haas M.R., Davidson J.A., Erickson E.F. (eds.), ASP Conf. Ser. 73, 395
Goebel J., Volk K., Walker H., et al., 1989, A&A 222, L5
Groenewegen M.A.T., 1993, A&A 271, 180
Groenewegen M.A.T., de Jong T., 1998, A&A 332, 25
Habing H.J., 1996, A&AR 7, 97
Hackwell J.A., 1972, A&A 21, 239
Hafner S., 1961, Z. Krist. 115, 331
Hashimoto O., 1994, A&AS 107, 445
Hess P.C., 1995, Rev. Min. 32, 145
Hofmeister A.M., Keppel E., Bowey J.E., Speck A.K., 2000, in Proceedings of the Conference "ISO Beyond the Peaks" 2-4 Feb. 2000, Spain, ESA SP-456, 200, p. 38
Houk N., Smith-Moore M., 1988, Michigan catalogue of Two-Dimensional spectral types for the HD stars, Vol. 4: -26 to -12 degrees, Michigan Spectral Survey

Hron J., Aringer B., Kerschbaum F., 1997, A&A 322, 280
Huss G.R., Fahey A.J., Gallino R., Wasserburg G.J., 1995, ApJ 430, L81
Iben I. Jr., Renzini A., 1983, ARA&A 21, 271
Ivezic Z., Knapp G.R., 1998, Am. Astron. Soc. Meet. 193, 22.05
Ivezic Z., Elitzur M., 1995, ApJ 445, 415
Jeong K.S., Winters J.M., Sedlmayr E., 1999, in: Le Bertre T., Lèbre A., Waelkens C. (eds.), Asymptotic Giant Branch Stars, IAU Symp. 191, 233
Justtanont K., Feuchtgruber H., de Jong T., et al., 1998, A&A 330, L17
Kerschbaum F., Hron J., 1992, A&A 263, 97
Kosaza T., Sogawa H., 1998, Ap&SS 255, 437
Kosaza T., Sogawa H., 1997, Ap&SS 251, 165
Kwok S., Volk K., Bidelman W.P., 1997, ApJS 112, 557
Little-Marenin I.R., Little S.J., 1990, AJ 99, 1173 (LML90)
Little-Marenin I.R., Stencel R E., Staley S.B., 1996, ApJ 467, 806
Lodders K., Fegley B. Jr., 1999, in: Le Bertre T., Lèbre A., Waelkens C. (eds.), Asymptotic Giant Branch Stars, IAU Symp. 191, 279
Mattei J.A., Foster G., Hurwitz L.A., et al., 1997, in Proceedings of the ESA Symposium "Hipparcos – Venice '97", p. 269
Monnier J.D., Geballe T.R., Danchi W.C., 1998, ApJ 502, 833
Monnier J.D., Geballe T.R., Danchi W.C., 1999, ApJ 521, 261
Morioka T., Kimura S., Tsuda N., et al., 1998, MNRAS 299, 78
Neri R., Kahane C., Lucas R., Bujarrabal V., Loup C., 1998, A&AS 130, 1
Nittler L.R., Alexander C.M.O'D., Gao X., Walker R.M., Zinner E.K., 1997, ApJ 483, 475
Nittler L.R., Alexander C.M.O'D., Gao X., Walker R.M., Zinner E.K., 1994a, Nat 370, 443
Nittler L.R., Alexander C.M.O'D., Gao X., Walker R.M., Zinner E.K., 1994b, Meteoritics Planet. Sci. 29, 512
Nuth J.A., Hecht J.H., 1990, Ap&SS 163, 79
Nyquist R.A., 1971, Infrared Spectra of Inorganic Molecules. Academic Press: New York
Onaka T., de Jong T., Willems F.J., 1989, A&A 218, 169
Pégourié B., Papoular R., 1985, A&A 142, 451
Posch T., Kerschbaum F., Mutschke H., et al., 1999, A&A 352, 609
Preudhomme J., Tarte P., 1971, Spectrochimica Acta 27A, 1817
Richards A.M.S., Yates J.A., Cohen R.J., 1999, MNRAS 306, 954
Richards A.M.S., 1997, Ph.D. Thesis
Salpeter E.E., 1974, ApJ 193, 579
Sedlmayr E., 1989, in Interstellar Dust, Allamandola L.J., Tielens A.G.G.M. (eds.), IAU Symp. 135, 467
Skinner C.J., Griffin I., Whitmore B., 1990, MNRAS 243, 78
Sloan G.C., LeVan P.D., Little-Marenin I.R., 1996, ApJ 463, 310
Sloan G.C., Price S.D., 1995, ApJ 451, 758 (SP95)
Sloan G.C., Price S.D., 1998, ApJS 119, 141 (SP98)
Speck A.K., 1998, Ph.D. Thesis
Stencel R.E., Nuth J.A., Little-Marenin I.R., Little S.J., 1990, ApJ 350, L45
Sylvester R.J., 1999, MNRAS 309, 180
Sylvester R.J., Barlow M.J., Skinner C.J., 1994, MNRAS 266, 640
Sylvester R.J., Barlow M.J., Skinner C.J., 1998, MNRAS 301, 1083
Tielens A.G.G.M., 1990, in From Miras to Planetary Nebulae: Which Path for Stellar Evolution? Proceedings of the International Colloquium, Montpellier, France. Gif-sur-Yvette, France: Éditions Frontières, p. 186
Treffers R., Cohen M., 1974, ApJ 188, 545
Triglio G., Umana G., Cohen R.J., 1998, MNRAS 297, 497
Tropf W.J., Thomas M.E., 1991, in Handbook of Optical Constants of Solids II, Palik E.D. (ed.). Academic Press, Boston, p. 883
Tsuji T., Ohnaka K., Aoki W., Yamamura I., 1997, Ap&SS 255, 293
Vardya M.S., de Jong T., Willems F.J., 1986, ApJ 304, L29
Water L.B.F.M., Beintema D.A., Cami J., et al., 1999, in The Universe as seen by ISO, Cox P., Kessler M.F. (eds.), ESA SP-427, 219
Whitelock P.A., 1986, MNRAS 219, 525
Woolf N.J., Ney E.P., 1969, ApJ 155, L181
Zachariasen W.H., 1932, J. Am. Chem. Soc. 54, 3841